THE UNIVERSITY OF MANITOBA

A DISTRIBUTED VORTEX THEORY FOR THE AUGMENTOR WING

by

VINH QUYEN TANG

A THESIS

SUBMITTED TO THE FACULTY OF GRADUATE STUDIES

IN PARTIAL FULFILLMENT OF THE REQUIREMENTS

FOR THE DEGREE OF MASTER OF SCIENCE

DEPARTMENT OF MECHANICAL ENGINEERING

WINNIPEG, MANITOBA

SEPTEMBER, 1974

A DISTRIBUTED VORTEX THEORY FOR THE AUGMENTOR WING

by

VINH QUYEN TANG

A dissertation submitted to the Faculty of Graduate Studies of the University of Manitoba in partial fulfillment of the requirements of the degree of

MASTER OF SCIENCE

THE UNIVERSITY OF MANITOBA

FACULTY OF GRADUATE STUDIES

The undersigned certify that they have read, and recommend to the Faculty of Graduate Studies for acceptance, a Master's thesis entitled: A distributed vortex theory for the augmentor wing

submitted by Quyen Vinh, TANG

in partial fulfilment of the requirements for the degree of Master of Science

J. Tinkler

Date September 20/74

Oral Examination is:

Satisfactory ☐ Not Required ☑

[Unless otherwise specified by the major Department, thesis students must pass an oral examination on the subject of the thesis and matters relating thereto.]

ABSTRACT

Experimental results in the past have revealed the encouraging aspect of the augmentor wing in the development of STOL. Although attempts have been made to predict the performance of the augmentor wing analytically, a satisfactory theory for augmentor wing has not yet been obtained. The present study is a further effort in this direction to provide a means to analyse the augmentor wing theoretically.

The two-dimensional augmentor wing was simplified to a flat plate aerofoil with the thick jet issuing at the trailing edge. Thin aerofoil theory was used and the aerofoil was replaced by a plane vortex distribution. The two-dimensional jet was substituted by two vortex distributions on its boundaries and a plane distributed source at the aerofoil trailing edge, between the two vortex sheets. Inviscid, incompressible flow was assumed in the main stream and in the jet, and the flow was everywhere irrotational except on the jet boundaries.

As a test the numerical method was applied to the simpler lifting system, the thin jet flap arrangement, where the jet thickness was assumed to approach zero and as a result there was only a single vortex distribution on the jet centre line.

The continuous vortex strength distributions on the aerofoil and on the jet were approximated by stepped constant-strength vortex distributions. The conditions that the aerofoil and the jet are streamlines and the known

relation between the local vortex strength and the jet curvature are satisfied alternately in an iterative process.

The iteration was normally divergent but a special technique was developed to yield convergence. The results for lift coefficient obtained were reasonably good compared to the experimental results and the analytical solution of the linearized jet flap problem. However, the pure stepped vortex distribution method did not provide an adequate representation of vortex strength distribution near singularities at the leading and the trailing edges. The method was modified by allowing the three vortex segments adjacent to the singularities to have logarithmic distributions. The result showed a better distribution of vortex strength.

The numerical method was then applied to the straight thick jet with zero attack and jet initial deflection angles. The result showed a close agreement to the analytical solution.

The work in this thesis has established that the vortex representation and the computing techniques form a reasonable method for obtaining a solution to the augmentor wing problem.

ACKNOWLEDGEMENTS

I would like to thank Dr. J. Tinkler for his helpful and patient guidance through the course of this work.

I also wish to express my appreciation to the staff of the Mechanical Engineering Department and to Miss Karen Kindraka who helped in typing this manuscript.

The financial aid from the Defence Research Board for the using of the computer is acknowledged.

TABLE OF CONTENTS

Page

LIST OF SYMBOLS

A	The constant associated with the logarithmic terms
c	Chord length
C_J	Jet momentum coefficient
C_L	Lift coefficient
J_m	Jet momentum flux
K_1, K_2	The constants of integrations
l_J	Jet length measured in chord-length
L	Total lift per unit span
N	Total number of vortex segments in the aerofoil and the jet
NC	Number of vortex segments in the aerofoil
NJ	Number of vortex segments in the jet
r	Distance from the vortex segment end point to the control point
R	Radius of curvature
S	Arc length
U	Mean main stream velocity near jet
u	x component of induced velocity
u'	ξ component of induced velocity
V	Mean jet velocity
v	y component of induced velocity
v'	η component of induced velocity
x	horizontal coordinate
y	vertical coordinate

y', y'' First and second derivative of y with respect to x

α Angle of attack

γ Vortex strength per unit length

Γ Circulation about the vortex segment

δ Jet thickness

ε Distance from the segment end point to the control point

η Normal axis to the vortex segment line

θ angle measured from the source distribution line to the line connecting its end point to the control point $(0 < \theta < 2\pi)$

λ $|\lambda| = |\psi|$ the angle formed from the vortex segment line & x axis

ν Strength per unit length of the doublet distribution

ξ Coordinate parallel to the vortex segment line

ρ Density

τ Initial jet deflection angle

ϕ Angle measured from the vortex segment line to the line connecting the segment end point to control point $(0 < \phi < 2\pi)$

ψ $\tan(\psi)$ is the slope of the aerofoil and the jet boundaries

LIST OF SUBSCRIPTS

c of the aerofoil

i order of control points

j order of vortex segments

J	of the jet
nc	of the last vortex segment in aerofoil
nj	of the first vortex segment in the jet
oj	initial conditions of a vortex segment
m, m+1	at the two ends of a vortex segment, in the direction of increasing x coordinate
s	of the source
∞	of the main stream far upstream of the aerofoil

LIST OF FIGURES

CHAPTER I

INTRODUCTION

Aerodynamically, the development of STOL (Short Take Off and Landing) aircraft resulted from step by step progress in the search for wings with high lift coefficients. The quest for high lift aerofoils started as early as 1920, however, it was not until 1952 that the solution of high lift wing emerged through the concept of the jet flap, in which the propulsive jet is ejected from a spanwise slot at the trailing edge of the wing. Its effectiveness depends upon the aerodynamic synthesis of the lifting and propulsive systems (Ref. 1).

In 1955, M. Davidson reported in Ref. 1 experiments on a two-dimensional jet flap, the basic idea of which was described as "to baulk the lower main stream, force it over the wing and so, following Bernouilli, aerodynamic lift is generated". The report was based mainly on the empirical theory of Stratford and experiments of Dimmock at the National Gas Turbine Establishment. The theory had made use of the idea of analogy to the mechanical trailing edge flap (Fig. 1), and the results showed, in principle, the possibility of attaining very high lift coefficients by means of a jet flap. Experiments were carried out on a two dimensional model of elliptic wing (Fig. 2) where lift and pitching moment were measured by pressure plotting. Results also showed that the propulsive thrust was nearly equal to the momentum flux of the jet regardless of the jet deflection angle.

A year later D. A. Spence (Ref. 2) presented a theoretical solution for the inviscid, incompressible flow past a thin, two dimensional aerofoil with an irrotational jet emerging at the trailing edge. Furthermore, due to the complexity of the integro-differential equations involved, the problem was solved only for the case of small incidence and jet-deflection angles. Useful results were obtained for pressure distribution, lift and pitching moment. It is worth noting the logarithmic expression in the solution, which correctly describes the singular behaviour of the flow at the trailing edge. Though the problem was linearized, the results have proved to be applicable to large jet-deflection angles.

The practicality of the jet flap lifting system was improved by ejecting the jet over a trailing-edge flap of moderate size, as seen in Fig. 3, instead of from the trailing edge. Spence (Ref. 3) presented the theory of lift for such a system known as a jet-augmented flap.

Almost a decade later, the jet-augmented flap arrangement was modified by adding a shroud to improve the lifting effectiveness. The latter arrangement is called an augmentor wing and is illustrated in Fig. 4. A jet issuing from a span-wise slot at the rear portion of an aerofoil emerges into a gap formed by the upper shroud and lower section of the flap, which direct the flow with a downward angle of deflection relative to the aerofoil chord. The flap is designed to allow mixing of the jet and the secondary induced air flow (Fig. 4) as a result, augmentation of momentum flux of the primary jet is obtained.

The arrangement of the augmentor wing contributes to high lift on two accounts: the presence of the jet induces an assymmetry in the main stream giving rise to a pressure lift on the aerofoil, and the

reaction of the augmented jet momentum results in a contribution to lift (as well as a contribution to thrust). The reaction lift is clearly an advantage over the jet flap arrangement.

Past augmentor wing investigations have been mainly laboratory experiments. In 1964, at Fourth ICAS Conference in Paris, Whittley (Ref. 4) presented a report on research progress which indicated the promise of the augmentor wing concept. Research work was then continued with tests on a large scale model in the NASA Ames 40 by 80 feet wind tunnel, and the results have shown a significant advantage of such a lifting system. In 1969, Y.Y. Chan (Ref. 5) contributed to the analytical solution of the augmentor wing by simplifying the model to that of a jet-augmented flap with sinks at the hinge line on upper or lower wing surfaces. The sink flow is combined with the jet flow to represent the augmentor action. He shows that the lift coefficient could be improved by augmentor wing arrangement.

The present work is an attempt to provide a better theoretical method for predicting the performance of the augmentor wing. Since the flow about an augmentor wing is very complex, this study will be based on a greatly simplified model. Also the thin aerofoil theory will be applied and the idea of replacing aerofoil and jet by vortex sheets will be adopted.

CHAPTER II

MATHEMATICAL MODEL OF AUGMENTOR WING

2.1 Introduction

The velocity field induced by a distributed vortex is a very important concept in aerofoil theory as discussed, for example, in Chapter 12 of Reference 6. The flow about a two-dimensional aerofoil can be represented by the flow resulting from the combination of a uniform stream with a distributed vortex, the actual strength distribution being determined by the shape of the aerofoil. The method provides a convenient means to determine not only the total lift but also the distribution of pressure on an aerofoil.

The problem of determining the aerodynamic coefficients of a given aerofoil profile is very difficult. However, M. Munk (Ref. 6) has introduced a method of approximation, known as the theory of thin aerofoil, which has proved to be very useful. The method replaces an aerofoil by its mean camber line which is assumed only slightly deviated from the chord line.

In addition to the use of vortex sheet and thin aerofoil theories, the simplification of the augmentor wing configuration will be taken systematically so that it is possible to solve the problem and to test its results at each stage, from the simplified case to the more complex one.

2.2 Idealized Models

The configuration of, and the flow about an augmentor wing are so complicated that major simplifications of the wing model is necessary for the study of augmentor wing.

The simplified two-dimensional augmentor wing model consists of a thin aerofoil with a downward deflected flap at the rear portion of the aerofoil and a parallel shroud just above the flap as shown in Fig. 5. The augmented jet is ejected between the shroud and the flap at the trailing edge in the direction of the flap chord line. Noting that without taking the effect of the shroud into consideration the problem of the augmentor wing is an extended case of the jet augmented flap, in which the jet thickness is finite and does not approach zero. The problem, thus, could be solved first by neglecting the effect of the shroud, the simplified model then becomes as sketched in Fig. 6, so that the results could be tested at the limiting case where jet thickness is approaching zero. Now, as an analogy to the step-by-step progress in the establishment of theory of lift for the thin two dimensional jet augmented flap (Ref. 2 and Ref. 3), before studying the model in Fig. 6, a more simplified model where the effect of the flap is neglected will be examined first. In this latest model, as shown in Fig. 7, the jet will be considered to be ejected from the trailing edge of a thin aerofoil. The model is simplified further by assuming that the aerofoil has no camber. The model is shown in Fig. 8 and consist of a flat plate at an angle of attack with a thick jet at the trailing edge. The work in this thesis is aimed at leading to a solution of a flat plate aerofoil with a thick jet.

It is desired now to use the concept of distributed vortices to construct a hypothetical model for the augmentor wing of Fig. 8. The flat plate is replaced by a distributed vortex with unknown strength along its line, and the jet is replaced by two vortex sheets at its boundaries and a source distribution at the trailing edge (Fig. 9), their strengths are to be determined.

The problem will be solved numerically by an iterative method. But first of all the problem of the thin jet flap will be solved to test the technique of iteration. The jet flap model is the limiting case of the augmentor wing of Fig. 9, as the jet thickness approaching zero. It consists of the vortex distributions along a flat plate and along the trajectory of the jet originated from the trailing edge (Fig. 10).

2.3 Straight Uniform Jet

In Chapter 3 of Reference 7, the technique of replacing two parallel vortices and a uniform flow by a source distribution is discussed. The technique is modified here to represent a jet by source and vortex distributions.

Here the two semi-infinite, parallel vortex distributions on two straight lines $y=\frac{\delta}{2}$ and $y=-\frac{\delta}{2}$, as shown in Fig. 11, are added to a source distribution on the y axis and between the two vortex distribution. It can be shown that if the source distribution has equal strength to the two vortex sheets, the resulting flow is a straight uniform flow in the region $x > 0$ and between the two vortex sheets (see Appendix G).

It is assumed, in this work, that the curved jet in a uniform flow can also be represented by vortex sheets and a source distribution of unknown strength distribution as shown in Fig. 9.

2.4 Thin Curved Jet

A curved, thin, two dimensional jet in a co-flowing external field is sketched in Fig. 12. Its trajectory is determined by the radius of curvature R of its centre line and the arc length S measured along its curve. The jet thickness δ, perpendicular to the centre line, varies along the jet.

The analysis following that of Spence, Reference 2, assumes an inviscid, incompressible flow in the main stream and in the jet, and the flow is everywhere irrotational except at the boundaries of the jet, where the pressure is continuous but the velocity and density are both discontinuous.

The velocity and the pressure at the centre line vary along the jet, they are fuctions of S; there remain only two independent physical quantities that are constant: the mass flow and the total pressure. A polar element of the jet is shown in Fig. 13. The vortex sheets at the two boundaries may be replaced by a single vortex sheet along the center line together with a doublet distribution. Spence's analysis (Ref. 2) is repeated in Appendix A where expressions result for the center line vortex distribution γ_J and doublet distribution ν, in terms of the jet properties and position. The expressions are:

$$\gamma_J = \frac{U}{R}\left[\frac{\rho V^2 \delta}{\rho_\infty U^2} - \delta\right], \tag{1}$$

and

$$\nu = U\delta\left[1 - \frac{\rho V^2 \delta^2}{4\rho_\infty U^2 R^2}\right] \tag{2}$$

where ρ_∞ and ρ are densities of air in the main stream and in the jet

respectively. Also U and V are the mean velocities of the main stream and the jet.

2.5 Extremely Thin, Curved Jet

An extremely thin, curved jet is defined as a curved jet at the limit where thickness is assumed to approach zero or $\delta \to 0$. Spence has analyzed the problem in Reference 2 by letting the mean velocity go to infinity but keeping the momentum flux finite. He found that, at the limit, the vortex strength distribution, equation (1), became

$$\gamma_J = \frac{U}{R} \frac{J_m}{\rho_\infty U^2} \tag{3}$$

where J_m is the momentum flux, $J_m = \rho V^2 \delta$. The doublet distribution, equation (2), vanishes.

2.6 Boundary Conditions

In using vortex sheets to represent the aerofoil and the jet, one of the physical condition needed in determining the strength of the vortex distribution is that there will be no flow across the aerofoil and the jet.

Generally, without knowing the type of vortex distribution, this condition means the vortex sheets should assume strength distributions that induce a velocity field such that the aerofoil and the jet are streamlines. Mathematically, the velocities induced by vortex sheets at any point on the boundary, when combined with the uniform flow velocity should make a velocity tangential with the boundary at that point, or

$$\frac{U_\infty \sin\alpha + v_i}{U_\infty \cos\alpha + u_i} = \tan(\psi_i) \quad , \tag{4}$$

where α is the angle of attack (Fig.14) and $\tan(\psi_i)$ is the slope of the streamline at ith control point. Also v_i and u_i are vertical and horizontal components of the induced velocity, and U_∞ is the main stream velocity.

CHAPTER III

STEPPED VORTEX DISTRIBUTION

(FOR THE THIN JET FLAP)

3.1 Equations

The continuous vortex distributions which are being used to represent the flat plate aerofoil and thin jet may be replaced by a large number of short segments of constant strength vortex sheets for the purpose of applying numerical methods for solving the problem.

The velocities induced at a point (i) by a constant strength vortex distribution (Fig. 15) are given by (see Appendix B)

$$v'_{i-j} = \frac{\gamma_j}{2\pi} \left(\ln \frac{r_{m+1}}{r_m}\right)_{i-j} \tag{5}$$

$$u'_{i-j} = \frac{\gamma_j}{2\pi} \left(\phi_{m+1} - \phi_m\right)_{i-j} \tag{6}$$

where v'_{i-j} and u'_{i-j} are η and ξ components, respectively, of induced velocity at ith control point by jth element of vortex distribution and subscripts m and m+1 denote the two ends of each distributed vortex segment in the direction of increasing ξ coordinate. It should be noted that positive ϕ is from the positive ξ-axis counter-clockwise to the line connecting the segment end to the control point, and the magnitude of ϕ is from 0 to 2π.

The induced velocity field of the vortex distributions when combined with the uniform flow field must give streamlines which include the

aerofoil and jet boundaries as special streamlines. The strengths of the vortex elements are determined by satisfying the set of equations (4) which are the boundary streamline conditions.

Rewriting (4) in terms of v_{i-j} and u_{i-j},

$$\sum_{j=1}^{N} v_{i-j} - \tan(\psi_i) \sum_{j=1}^{N} u_{i-j} = U_\infty [\tan(\psi_i) \cos\alpha - \sin\alpha] \qquad (7)$$

Where N is the total number of elements of vortex distribution. By substituting (5) and (6) into (7),

$$\sum_{j=1}^{N} \frac{\gamma_j}{2\pi} \left[\left(\ln \frac{r_{m+1}}{r_m}\right)_{i-j} - \tan(\psi_i) \left(\phi_{m+1} - \phi_m\right)_{i-j}\right] =$$

$$U_\infty [\tan(\psi_i) \cos\alpha - \sin\alpha]. \qquad (8)$$

If N control points(i) are taken on the aerofoil and jet, equation (8) gives sufficient linear simultaneous equations to determine the N values of γ_j for a given jet shape. The choice of the N control points will be discussed later.

3.2 Iterative Method of Solution

3.2.1 General Principles of the Method

The equations of section 3.1 assume that the location of the vortex elements is known. In the problem being solved, the location of the jet vortex distributions is not known. The iterative solution being proposed assumes an initial jet shape and uses equation (8) to determine the vortex strength distribution. Then the vortex strength distribution is used to predict the jet shape from its initially specified slope and its curvature (given by equation (3)). The new shape is then

used as the basis of a second calculation of vortex strength distribution and jet shape. The process is iterative until the shape shows no further change.

3.2.2 Geometrical Construction of the Problem

First the chord line and the jet trajectory is divided into a chosen number of finite length segments, which are approximated to the straight lines as shown in Fig. 16, and a constant strength distributed vortex is assumed on each segment. Since a large number of segments taken will result in more unknown vortex strengths to be determined, it would result in longer computing time. Thus, for better approximation of vortex strength distribution with less computing time the segment lengths may vary according to the behaviour of the distribution. Shorter segments are used in the regions of rapidly changing strength (i.e. adjacent to the singularities of the vortex distribution), and longer segments are used when the vortex strength does not change significantly.

Now, a number of control points on the chord and the jet is established equal to the number of segments taken. At these control points the induced velocities are caused to satisfy the boundary conditions at the aerofoil and jet by applying the set of equation (8). Normally, control points would be chosen at the middle of the elements. This was tried and produced a solution in which the vortex strength of elements fluctuated in sign. This is contrary to physical reasoning and Spence's linearized solution and can be explained as follows.

Consider a flat plate aerofoil at zero angle of attack, the lift being due to the jet flow. The velocity normal to the aerofoil must be zero. Now consider the velocity normal to the first (leading edge)

element of the aerofoil. There is no contribution from the main stream. The constant strength vortex distribution of the first element itself induces upward velocities over the front half and downward velocities over the rear half and zero at the mid point, where, however, all the following vortex elements (which must be all of positive sign) induce upward velocities. Thus it is physically impossible to attain zero normal velocity at mid point of the first element.

Therefore control points are taken on each segment towards the downstream end as shown in Fig. 16, at a distance (ε/c) from the downstream end.

3.2.3 Computing the Solution

The three main steps involved in each iteration are the computing of the vortex distributions from a given jet shape, the computing of the jet shape from the calculated vortex distribution and, finally, the process of adjusting the jet shape for the input to the next iteration. The Flow Chart of the computer progam is in Appendix C.

Step 1 In computing the vortex strength for each segment, it is necessary to calculate r_m, r_{m+1} and ϕ_m, ϕ_{m+1} in the set of equations (8) to form a coefficient matrix. From Fig. 15

$$r_m^2 = (\xi_i - x_m)^2 + (\eta_i - y_m)^2 \tag{9}$$

$$r_{m+1}^2 = (\xi_i - x_{m+1})^2 + (\eta_i - y_{m+1})^2 \tag{10}$$

and

$$\phi_{m+1} - \phi_m = \text{Arctan } \left(\frac{\eta_i - y_{m+1}}{\xi_i - x_{m+1}}\right) - \text{Arctan } \left(\frac{\eta_i - y_m}{\xi_i - x_m}\right) \tag{11}$$

It should be noted that when the distributed vortex segment is not parallel to the x-axis, the induced velocities found by using formulas (5) and (6) have to be transferred to the vertical and horizontal components of the x-y coordinate system defined in Fig. 15 by

$$\begin{bmatrix} \cos(\lambda) & \sin(\lambda) \\ -\sin(\lambda) & \cos(\lambda) \end{bmatrix} \begin{bmatrix} u'_{i-j} \\ v'_{i-j} \end{bmatrix} = \begin{bmatrix} u_{i-j} \\ v_{i-j} \end{bmatrix}$$

where λ is the angle measured from the segment to the x axis with positive counter-clockwise, and u'_{i-j} and v'_{i-j} are the induced velocity components in the coordinate system where the ξ axis is parallel to the segment.

The slopes of the aerofoil and jet at each control point are also found to form a column matrix in the right hand side of the set of equation (8). The slope at each control point is assumed to be the same as that of the segment containing the point, thus

$$\tan(\psi_i) = \frac{\eta_m - \eta_{m+1}}{\xi_m - \xi_{m+1}} . \qquad (12)$$

The triangular elimination technique is then used to solve the set of linear, simulteneous equations (8) for the vortex strength distributions.

Step 2 The next computation is the determination of the jet slope for the vortex distributions just calculated. This is done by solving equation (3) for the jet curvature and thence computing the deflection. Equation (3) can be rewritten as

$$\gamma_J = \frac{UC_J}{2R} \qquad (13)$$

where C_J is the momentum coefficient,

$$C_J = \frac{J}{\frac{1}{2}\rho_\infty U_\infty^2} .$$

The radius of curvature of the jet, R, can be related to the first and second derivatives of the jet centre line and, approximating U to U_∞ (which is valid for small disturbance theory), equation (13) becomes

$$\gamma_J = \frac{U_\infty C_J}{2} \frac{y''}{(1 + y'^2)^{3/2}} . \tag{14}$$

For γ_J constant, the differential equation (14) can be easily solved as shown in Appendix D, and the jet shape is given by

$$y = -\frac{U_\infty C_J}{2\gamma_J} \left[1 - \left(\frac{2\gamma_J}{U_\infty C_J} x + K_1\right)^2\right]^{\frac{1}{2}} + K_2 \tag{15}$$

with the constants K_1 and K_2 being determined by

$$K_1 = \frac{y'_{oj}}{(1 + y'^2_{oj})^{\frac{1}{2}}} - \frac{2\gamma_J}{U_\infty C_J} x_{oj}, \tag{16}$$

and

$$K_2 = y_{oj} + \frac{U_\infty C_J}{2\gamma_J} \left[1 - \left(\frac{2\gamma_J}{U_\infty C_J} x_{oj} + K_1\right)^2\right]^{\frac{1}{2}} \tag{17}$$

The subscript oj denotes the initial conditions of each distributed vortex segment, e.g. for the jet segment adjacent to the trailing edge, y_{oj} is the y coordinate of the trailing edge and y'_{oj} is the initial jet deflection slope.

Step 3 The normal iterative procedure would not have a Step 3 -

the jet shape resulting from Step 2 would be the input for Step 1 of the next iteration. The result of trying this simple procedure is illustrated by the jet shapes produced by successive iterations as shown in Fig. 17. The iterations diverge. Step 3 is introduced in order to induce a convergence. It is seen from Fig. 17 that the first assumed shape and the result of the first iteration should form an envelope setting upper and lower limits for the jet shape. The correct shape should be somewhere between the limits. Step 3 consists of specifying an intermediate shape for the input to Step 1 of the next iteration. The details of Step 3 are given in Appendix E.

3.2.4 Lift Coefficient

A short computation of lift coefficient is also included in the computer program. By definition, the lift coefficient is expressed as

$$C_L = \frac{L}{\frac{1}{2}\rho_\infty U_\infty^2 c} \tag{18}$$

where c is the aerofoil chord length, taken to be unit here, and L is the total lift (per unit span).

$$L = \rho_\infty U_\infty \sum_{j=1}^{N} \Gamma_j \tag{19}$$

where Γ_j is the circulation about jth segment

$$\Gamma_j = \int_{x_m}^{x_{m+1}} \gamma_j dx = \gamma_j \, (x_{m+1} - x_m) \tag{20}$$

Thus the lift coefficient becomes

$$= \frac{2}{U_\infty} \sum_{j=1}^{N} \gamma_j \, (x_{m+1} - x_m) \tag{21}$$

3.3 Analysis of the Effects of Finite Jet Length and Finite Number of Distributed Vortex Segments

Because of computing limitations, the jet-flap solution will be determined by a finite number of distributed vortex segments and for a finite jet length only. Thus, it is necessary to test the effect on accuracy of these variables - the number of distributed vortex segments and the length of the jet.

The testing was carried out for the lifting system with zero angle of attack, the initial jet deflection angle of -31.4^{o} and the jet momentum coefficient of 2.0 ($C_J = 2.0$). ε was taken as 0.015c. It should be mentioned that segments in the aerofoil and in the jet are taken to be of equal lengths because the varying of the segment lengths in these regions would contribute insignificant advantage in this case where the number of segments used are not very large. Also, the lift coefficient, because of its practical significance and its sensitivity, will be used to gauge the effect of the other variables.

3.3.1 The effect of number of segments in aerofoil on the lift coefficient

A test was run with the number of segments in the aerofoil changing while other input variables were kept constant. The jet length was taken to be three-chord lengths downstream and divided into twelve segments. The results are shown in Fig. 18. The lift coefficients are almost constant for the cases of 3, 5, 7, 9 and 11 aerofoil segments and show the independence of the lift coefficient from the number of distributed vortex segments taken in aerofoil.

3.3.2 The effect of number of segments in the jet on the lift coefficient

Fig. 19 presents the changing of lift coefficient with respect to the number of segments taken in the jet. The jet length was three chord-length downstream and 3 segments of distributed vortex were taken in the aerofoil. The results show that the lift coefficient attains the asymptotic value after the number of segments taken in the jet becomes larger than 20.

3.3.3 The effect of jet length on the lift coefficient

While keeping the jet momentum, the attack and the jet deflection angles and the number of segments in the aerofoil constant ($N_C = 3$), the program was run to compute the lift coefficients for different lengths of the jet. Results shown in Fig. 20 illustrate the insignificant effect on lift coefficient of the part of the jet which is at more than four-chord lengths from where the jet issued.

3.4 Solutions and Discussions

Another factor which has effect on the solution is the position of control points. A test was run with variable values of ε, and the convergence of the jet shape is recorded in Fig. 21. It shows that at zero angle of attack and with the initial jet angle of -31.4° and the jet momentum coefficient of 2.0 and also with the number of segments of 11 in aerofoil and 12 in the jet, the jet shape gets closer to Spence's solution as ε/c increases from 0.005 to 0.010 but increasing ε/c to 0.015 causes no further change. It was found from preliminary computations that if ε was such that the control point was at the middle of the vortex distribution segments, the vortex strength became unrealistic. Therefore

very large values of ε should not be used. The value of $\varepsilon = 0.015c$ has been used for subsequent calculations. The difference between the present jet shapes and that predicted by Spence is attributed to the linearizing technique used by Spence. (He assumed the jet to be very close to the aerofoil chord line).

Results of vortex distributions and the corresponding jet shape are illustrated in Fig. 22 and Fig. 23 for the same attack and initial jet deflection angles but different values of jet momentum coefficients, $C_J = 2.0$ and $C_J = 4.0$ respectively. In both cases the jet shapes obtained are quite close to Spence's results of Reference 2 but both shapes are lower than those of Spence. Also the stepped functions found for the vortex distributions represent the trend of the varying of vortex strength along the aerofoil and the jet. Particularly in the region free from singularities which are at x=0 and x=1 in Fig. 22 and Fig. 23 the results are quite close to Spence's solutions which were proved to be close to experimental results (Ref. 2).

The lift coefficient as a function of the attack angle is computed and compared to Spence's results. Calculations over the angle of attack range from -10^{o} to 10^{o} show the almost linear relation between the lift coefficient and the attack angle (Fig. 24), but the lift coefficients found are lower than predicted by Spence.

The variation of lift coefficient with momentum coefficient is shown in Fig. 25 to be close to the results of Spence and the experimental results of Reference 8. The present results are closer to the other works for low jet momentum coefficients.

From these results, for further calculations it is reccommended

that 20 segments are taken in the jet with its length being four chord-lengths downstream, and the number of segments in the aerofoil could be as low as 3 if the only interest is in lift coefficient, or not less than 11 if vortex strength distribution is concerned. Also ϵ should be taken at 0.015c.

CHAPTER IV

MODIFIED STEP VORTEX DISTRIBUTION

(FOR THE THIN JET FLAP)

4.1 Treatment near singularities at the leading and trailing edges

For a better approximation of vortex strength distribution which could more correctly describe the singular behaviour of the flow at the leading and trailing edges, a modification of the previous stepped function is introduced.

Spence has found the reasonable logarithmic terms which satisfy the physical condition of the flow at the trailing edge, and give the singularities required. In the modified step function method these logarithmic terms are applied to the first element of vortex distribution at the leading edge and to the two elements adjacent to the trailing edge.

The logarithmic terms applied to elements on the aerofoil and the jet are

$$\gamma_1 = A_1 \frac{\ln (1-x)}{x^{3/2}} ,$$

$$\gamma_{nc} = A_{nc} \frac{\ln (1-x)}{x^{3/2}} ,$$

$$\gamma_{nj} = A_{nj} \frac{\ln (x-1)}{x^{3/2}} ,$$

for the aerofoil leading edge, aerofoil trailing edge and the first jet element respectively. The constants, A, have to be determined from

equation (7) which becomes

$$\sum_{\substack{j=2 \\ j\neq NC \\ j\neq NJ}}^{N} \frac{\gamma_j}{2\pi} \left[\left(\ln \frac{r_{m+1}}{r_m}\right)_{i-j} - \tan(\psi_i) \left(\phi_{m+1} - \phi_m\right)_{i-j} \right] +$$

$$\frac{A_1}{2\pi} \left[v_{i-1} - \tan(\psi_i)\, u_{i-1} \right] + \frac{A_{nc}}{2\pi} \left[v_{i-nc} - \tan(\psi_i)\, u_{i-nc} \right] +$$

$$\frac{A_{nj}}{2\pi} \left[v_{i-nj} - \tan(\psi_i)\, u_{i-nj} \right] = U_\infty [\tan(\psi_i) \cos\alpha - \sin\alpha] \tag{22}$$

The induced velocities v_{i-1}, v_{i-nc}, v_{i-nj} and u_{i-1}, u_{i-nc}, u_{i-nj} are readily found from equations (B.1) and (B.2) modified to allow for variable γ. For instance

$$v_{i-1} = -A_1 \int_{x_m}^{x_{m+1}} \frac{\ln(1-x)}{x^{3/2}} \frac{x_i - x}{(x_i-x)^2 + y_i^2}\, dx, \tag{23}$$

$$u_{i-1} = A_1 \int_{x_m}^{x_{m+1}} \frac{\ln(1-x)}{x^{3/2}} \frac{y_i}{(x_i-x)^2 + y_i^2}\, dx. \tag{24}$$

Now the set of equations (22) satisfied at N control points can be established and a set of linear equations with the unknowns consisting of the coefficients of the logarithmic terms and the constant vortex strengths of other elements is obtained.

4.2 Iterative Method of Solution

The geometrical construction of the problem and the basic steps of iteration are the same as what was described in Section 3.2 for the case of a pure stepped function of vortex distribution. However, in com-

puting the elements of the coefficient matrix of the equation (22), some additional numerical integrations are needed to handle the singularities. The integrations which are of the types described in equations (23) and (24) are first treated to remove the singularities in the intergrands as shown in Appendix F and then solve by the Gaussian Quadrature method.

4.3 Results and Discussions

The modified stepped function method was used to determine the vortex strength distribution for the case where the momentum coefficient was 4.0, the attack and the jet deflection angles were 0 and -31.4^{o} respectively and 15 segments of distributed vortex were taken. The resulting vortex distributions are as shown in Fig. 26. The result presents acceptable behaviours of vortex strengths at the singularities, which are comparable to Spence's results. Also the jet shapes shown in Fig. 27 were found for the same initial conditions but with C_J being 2 and 4. The jet shapes found are very close to what Spence predicted.

Lift coefficients were computed for the lifting system with zero attack angle, the jet deflection angle of -31.4^{o} and momentum coefficient being 1.0, 2.0, 3.0 and 4.0 successively. The results as seen in Fig. 28 show small difference in lift coefficients calculated by pure stepped function and modified stepped function methods.

It should be mentioned that there was another numerical solution using the discrete vortex distribution presented by Herold in Reference 9, the result of lift coefficient showed close agreement with Spence's of Reference 2, but the method does not approach to the treatment of singularities at the leading and trailing edges.

CHAPTER V

THICK JET

The step function method was applied in Chapter III and yielded good results for the thin jet flap problem. It is attempted now to use the same method to solve the thick jet case, the mathematical model of which was presented in Fig. 9. Vortex strength distributions on the aerofoil and on the upper and lower boundaries of the jet are assumed to be step functions which are to be determined, but the source distribution at the trailing edge is a uniform distribution with the strength related to the jet momentum coefficient. The jet thickness will be assumed constant to simplify the problem.

The computer program of the thick jet problem will be first tested to solve the special case of zero attack angle and with the thick jet of zero initial deflection angle. Then the thick curved jet problem will be attempted.

5.1 Equations of Streamline Conditions

The streamline boundary equation (4) of the jet flap is modified by including the induced velocities of the source distribution to satisfy the boundary conditions of the thick jet, and becomes

$$\frac{U_\infty \sin\alpha + \sum_{j=1}^{N} v_{i-j} + v_{i-s}}{U_\infty \cos\alpha + \sum_{j=1}^{N} u_{i-j} + u_{i-s}} = \tan(\psi_i) \qquad (25)$$

where u_{i-s} and v_{i-s} are the two components of velocity induced at the

point i by the source distribution and are given by equations (C.15) and (C.17) respectively. Rewriting equation (25) and substituting the expressions for induced velocities to give

$$\sum_{j=1}^{N} \frac{\gamma_j}{2\pi} \left[\left(\ln \frac{r_{m+1}}{r_m} \right)_{i-j} - \tan(\Psi_i) (\phi_{m+1} - \phi_m)_{i-j} \right] =$$

$$U_\infty [\tan(\Psi_i)\cos\alpha - \sin\alpha] + \frac{q}{2\pi} [(\theta_1 - \theta_2)\tan(\Psi_i) - \ln \frac{r_2}{r_1}] \qquad (26)$$

Equation (26) is the streamline condition of the thick jet, and when satisfied at N control points provides a set of linear, simultaneous equations with the N unknown vortex strengths to be determined.

5.2 Straight Thick Jet in Uniform Flow

The mathematical model of flat plate aerofoil with straight thick jet of zero attack and zero jet deflection angles is shown in Fig. 29; the lower jet boundary is on the x axis and the upper boundary is parallel to it and at a distance of δ (the jet thickness). The geometrical construction of the problem is similar to that discussed in Section 3.2 except for the jet part where the vortex segments are on both lower and upper jet boundaries instead of in a single boundary. Also the positions of control points are taken differently as shown in Fig. 29 which will be discussed later.

Two tests were run to determine the vortex strength distributions (in terms of the uniform source distribution strength) with the straight thick jet shape being treated as fixed. The jet length was taken as 9 chord-lengths with 12 distributed vortex segments (N_J=12), the segment lengths were each equal to a chord length except the last segments which

were four chord lengths. The jet thickness was 0.01 (δ=0.01).

The first test used control points at ε=0.015 upstream of the end points of each segment. The resulting values of γ/q were of fluctuating sign and magnitude. The reason for this erratic behaviour was traced to the finite length of the jet which was necessary for the numerical solution. When the control points are not far upstream of the downstream segments of the jet, the values of r_{11}, r_{22} (Appendix G) do not have a ratio of unity as would be the case for a jet stretching to infinity. It was therefore argued that the control points should all be sufficiently far upstream in the jet for this effect to be negligible. The N control points were chosed as shown in Fig. 29. The result of vortex strength distribution, recorded in Fig. 29, are comparable, with an exception of the last two pairs of vortex segments, to the analytical results which expects zero strength of vortex distribution on aerofoil and $\frac{\gamma}{q} = +1, -1$ on the lower and upper boundaries of the jet respectively (the reason for $\gamma = \pm 1$ is derived from the result of Appendix G).

CHAPTER VI

CONCLUSION

An attempt to solve the augmentor wing problem numerically has been made with the assumptions of inviscid, incompressible flow in the main stream and in the jet and irrotational flow everywhere except on the jet boundaries.

For the numerical solution it was necessary to assume a finite length for the jet. The vortex distribution was approximated by a finite number of segments of constant vortex strength. The boundary conditions which had to be satisfied were that the aerofoil and jet boundaries should be streamlines and the jet curvature had a definite relation to the local strength of the jet vortex distribution. These conditions required an iterative method of solution.

The numerical method was applied to the thin jet case and the results compared with the linearized solution of Spence. When vortex segments of constant strength were used it was found that a jet length of four chords was adequate. Eleven segments in the aerofoil and 20 in the jet gave a reasonable representation of the vortex distribution. A smaller number of segments gave a good prediction of lift coefficient.

A deficiency of the stepped vortex distribution method was that it did not give adequate representation of the singular behaviour of the vortex strengths at the leading and trailing edges. The method was modified by allowing the three segments adjacent to the singularities to

have logarithmic distributions. The modified step distribution method gave better representation of the vortex distributions over the aerofoil and jet.

Compared with Spence's results, the present method predicts a lower trajectory for the jet. This is attributed to the linearizing assumptions in Spence's theory. Herold's non-linearized method also gave a lower trajectory for small values of momentum coefficient.

The lift coefficients calculated at C_J values of 2 and 4 show a linear increase as the angle of attack increases from -10^o to 10^o. The present method gives lower values of C_L than either Spence's theory or the experimental results of Reference 8, but no conclusions can be drawn at present.

The first application of the numerical solution to the thick jet problem was to a simple straight jet. Excellent agreement was obtained with the exact solution.

It is finally concluded that the modified step method has been developed ready to apply to the thick curved jet of the augmentor wing problem.

APPENDICES

APPENDIX A

ANALYSIS OF A TWO DIMENSIONAL, JET POLAR ELEMENT

Consider a two dimensional polar element of the jet whose boundaries are treated as concentric, substending an angle $d\psi$ at its centre of curvature (Fig. 13). The pressures p_1 and p_2 at the upper and lower jet boundaries are continuous across the boundaries: total pressures are constant in the main flow and in the jet. Thus,

$$P_1 + \tfrac{1}{2} \rho_\infty U_1^2 = P_2 + \tfrac{1}{2} \rho_\infty U_2^2, \tag{A.1}$$

$$P_1 + \tfrac{1}{2} \rho V_1^2 = P_2 + \tfrac{1}{2} \rho V_2^2, \tag{A.2}$$

where U_1 and U_2 are main stream velcities just outside the upper and lower boundaries; the jet velocities inside the boundaries are, similarly, V_1 and V_2. Also, ρ_∞ and ρ are densities of air in main stream and in the jet respectively. Equation (A.1) and (A.2) are combined to yield

$$U_1^2 - U_2^2 = \frac{\rho}{\rho_\infty} (V_1^2 - V_2^2) \tag{A.3}$$

Since the flow is irrotational,

$$V_1 (R - \tfrac{1}{2}\delta) d\psi = V_2 (R + \tfrac{1}{2}\delta) d\psi \tag{A.4}$$

Introduce mean velocities to the flow inside the jet and the main stream, respectively

$$V = \tfrac{1}{2}\,(V_1 + V_2), \tag{A.5}$$

$$U = \tfrac{1}{2}\,(U_1 + U_2). \tag{A.6}$$

Now, equation (A.4) may be written as

$$V_1 - V_2 = \frac{V\delta}{R}, \tag{A.7}$$

and (A.3) as

$$U_1 - U_2 = \frac{\rho}{\rho_\infty}\,\frac{V^2\delta}{UR}. \tag{A.8}$$

Also, (A.2) may be rearranged to give

$$P_1 - P_2 = -\rho\,\frac{V^2\delta}{R} \tag{A.9}$$

Equation (A.8) gives the relation between main stream velocities, jet velocity, thickness and curvature. It is desired now to examine the vorticity distributions on the boundaries, which, while replacing the jet, have the same effect on the external flow.

The strengths of the elementary vortices, $\gamma_1\,ds_1$ and $\gamma_2\,ds_2$ (where s_1 and s_2 are arc lengths measured along the upper and lower boundaries) are

$$\gamma_1\,ds_1 = -U_1\,(R - \tfrac{\delta}{2})\,d\psi, \tag{A.10}$$

and

$$\gamma_2\,ds_2 = U_2\,(R + \tfrac{\delta}{2})\,d\psi \tag{A.11}$$

measured positive clockwise. They are equivalent to a single vortex of strength

$$\gamma_J ds = \gamma_1\,ds_1 + \gamma_2\,ds_2 \tag{A.12}$$

located along the jet center line, and a doublet of strength.

$$\gamma \, dS = \tfrac{1}{2} \, \delta \, (\gamma_1 \, dS_1 - \gamma_2 \, dS_2) \tag{A.13}$$

with its axis along the center line. On substituting (A.10) and (A.11) into (A.12), the strength of the single vortex becomes

$$\gamma_J dS = -U_1 \, (R - \tfrac{\delta}{2}) d\psi + U_2 \, (R + \tfrac{\delta}{2}) d\psi, \tag{A.14}$$

or

$$\gamma_J dS = -(U_1 - U_2) R \, d\psi + (U_1 + U_2) \, \tfrac{\delta}{2} \, d\psi. \tag{A.15}$$

Simplifying (A.15) by using the relation, $dS = -R \, d\psi$, gives

$$\gamma_J = (U_1 - U_2) - (U_1 + U_2) \, \frac{\delta}{2R} \tag{A.15}$$

Using (A.6) and (A.8) with (A.15) gives a more useful expression for γ_J,

$$\gamma_J = \frac{U}{R} \left[\frac{\rho V^2 \delta}{\rho_\infty U^2} - \delta \right], \tag{A.17}$$

Similarly, the expression for the doublet strength is found to be

$$\nu = U \, \delta \left[1 - \frac{\rho V^2 \delta^2}{4 \rho_\infty U^2 R^2} \right] \tag{A.18}$$

Equations (A.17) and (A.18) express the vortex and doublet strength as functions of the jet properties and position.

It is desired now to modify these expressions to apply to the limiting case where the jet thickness is assumed to approach zero, mean velocity goes to infinity but momentum flux remains finite.

Suppose $J_{m\infty}$, V_∞ and P_∞ are the momentum flux, the mean velocity

and the mean pressure in the jet at infinity and $J_{m\infty}$, V and P are those at any other point. If Q is the jet mass flow per unit span, then

$$Q = \rho V \delta = \rho V_\infty \delta_\infty \tag{A.19}$$

where δ_∞ is the jet thickness at infinity. The momentum flux can be expressed in term of Q as

$$J_m = QV \text{ and } J_{m\infty} = Q\, V_\infty. \tag{A.20}$$

Thus, from (A.20)

$$\frac{J_m - J_{m\infty}}{J_{m\infty}} = \frac{V - V_\infty}{V_\infty}. \tag{A.21}$$

Since the total pressure in the jet is constant,

$$\frac{1}{2}\rho\,(V^2 - V_\infty{}^2) = P_\infty - P,$$

or

$$V - V_\infty = \frac{2(P_\infty - P)}{\rho(V + V_\infty)}. \tag{A.22}$$

Upon substituting (A.22) into (A.21) and rearranging

$$\frac{J_m}{J_{m\infty}} = 1 + 2\,\frac{P_\infty - P}{\rho V_\infty (V + V_\infty)}. \tag{A.23}$$

But $P_\infty - P$ is also the pressure difference in the main stream, and hence proportional to $\frac{1}{2}\rho_\infty U^2{}_\infty$, thus,

$$\frac{J_m}{J_{m\infty}} = 1 + 0\,\left(\frac{U_\infty{}^2}{V_\infty{}^2}\right). \tag{A.24}$$

At the limit where the jet mean velocity becomes infinite ($V_\infty \to \infty$) and the momentum flux remains finite, it is deduced from (A.24) that

$$J_m = J_{m\infty} \tag{A.25}$$

or the momentum flux is constant along the jet. Also from (A.19) and (A.20)

$$Q = \frac{J_m}{V} \to 0, \quad \delta = \frac{J_m}{\rho V^2} \to 0 \tag{A.26}$$

Thus, the expression for vorticity distribution, equation (A.17), becomes

$$\gamma_J = \frac{U}{R}\left(\frac{J_m}{\rho_\infty U^2}\right) \tag{A.27}$$

and the doublet equation, equation (A.18), vanishes.

APPENDIX B

INDUCED VELOCITIES BY A TWO DIMENSIONAL STRAIGHT UNIFORM VORTEX DISTRIBUTION

Velocities induced by a straight uniform vortex distribution are derived in Reference 6 and summarized below.

Consider a uniform vortex distribution, whose strength is γ, along the x axis from $A(x_1,0)$ to $B(x_2,0)$ as in Fig. 15. Induced velocity components at P are:

$$v'_{i-j} = -\frac{\gamma}{2\pi} \int_{\xi_m}^{\xi_{m+1}} \frac{\cos(\phi)}{r}\, d\xi, \tag{B.1}$$

$$u'_{i-j} = \frac{\gamma}{2\pi} \int_{\xi_m}^{\xi_{m+1}} \frac{\sin(\phi)}{r}\, d\xi. \tag{B.2}$$

But $$r^2 = (\xi_i - \xi)^2 + \eta_i^2 \tag{B.3}$$

Differentiating both sides gives

$$2r\, dr = -2\,(\xi_i - \xi)\, d\xi \tag{B.4}$$

and hence

$$\cos(\phi)d\xi = \frac{\xi_i - \xi}{r}\, d\xi = -dr \tag{B.5}$$

Also differentiation of $\tan\phi = \dfrac{\eta_i}{\xi_i - \xi}$ gives

$$\frac{d\phi}{\cos^2\phi} = \frac{\eta_i d\xi}{(\xi_i - \xi)^2}\,, \tag{B.6}$$

so that

$$\sin\phi \, d\xi = \frac{\eta i}{r} \, d\xi$$

$$\sin\phi \, d\xi = \frac{(\xi_i - \xi)^2}{r \cos^2\phi} \, d\phi = r \, d\phi \tag{B.7}$$

By substituting (B.5) and (B.7) into (B.1) and (B.2) the induced velocity components become

$$v'_{i-j} = \frac{\gamma}{2\pi} \int_{r_m}^{r_{m+1}} \frac{dr}{r} = \frac{\gamma}{2\pi} \ln \frac{r_{m+1}}{r_m}, \tag{B.8}$$

$$u'_{i-j} = \frac{\gamma}{2\pi} \int_{\phi_m}^{\phi_{m+1}} d\phi = \frac{\gamma}{2\pi} (\phi_{m+1} - \phi_m) \tag{B.9}$$

u'_{i-j} and v'_{i-j} can be resolved into x and y components respectively by using the coordinate transformation

$$\begin{bmatrix} \cos(\lambda) & \sin(\lambda) \\ -\sin(\lambda) & \cos(\lambda) \end{bmatrix} \begin{bmatrix} u'_{i-j} \\ v'_{i-j} \end{bmatrix} = \begin{bmatrix} u_{i-j} \\ v_{i-j} \end{bmatrix}$$

where the angle λ, and u_{i-j} and v_{i-j}, two components of induced velocities, are as shown in Fig. 15.

APPENDIX C

FLOW CHART OF ITERATIVE SOLUTION METHOD

(THIN JET)

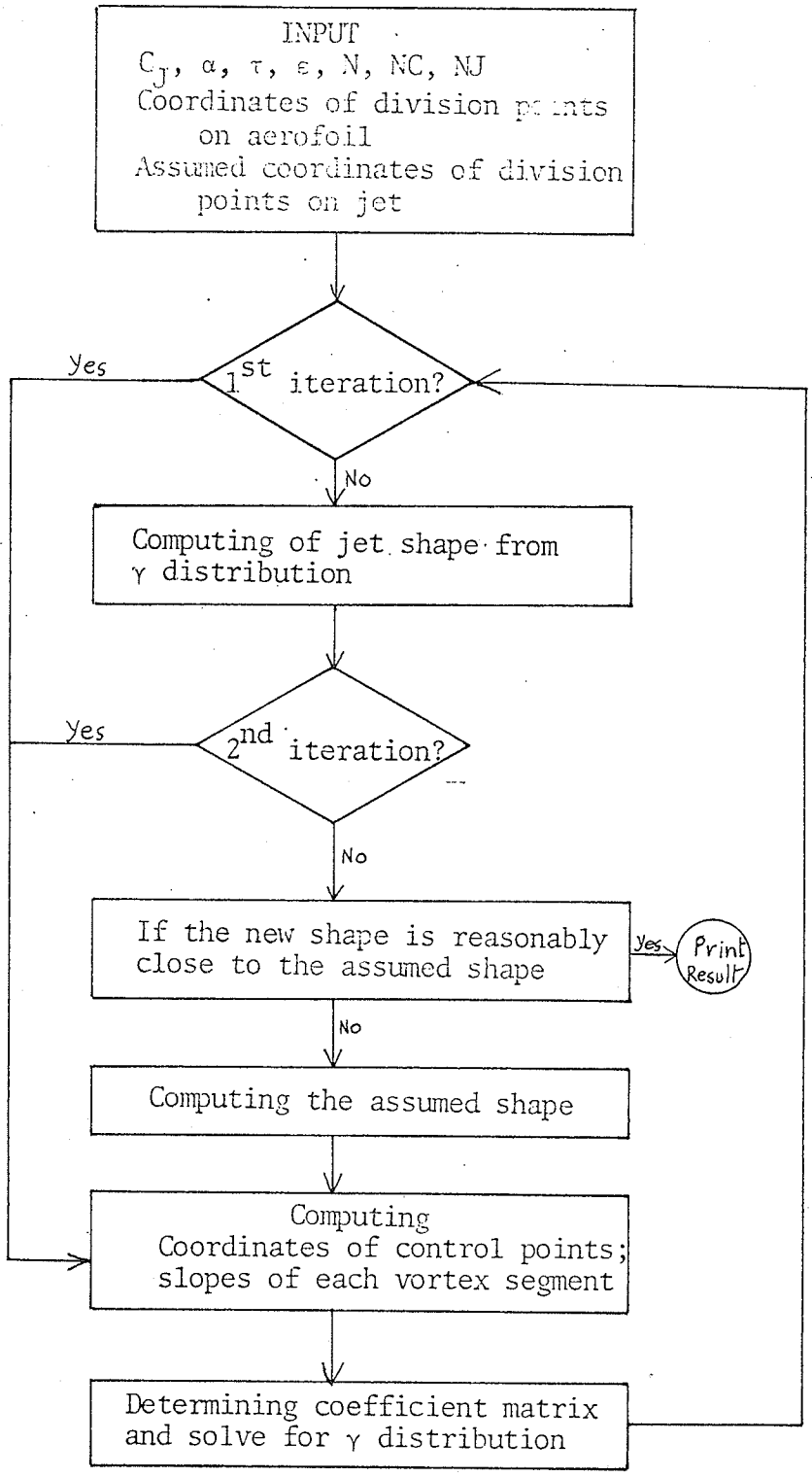
INPUT
C_J, α, τ, ε, N, NC, NJ
Coordinates of division points on aerofoil
Assumed coordinates of division points on jet
1st iteration?
Yes
No
Computing of jet shape from γ distribution
2nd iteration?
Yes
No
If the new shape is reasonably close to the assumed shape
Yes
Print Result
No
Computing the assumed shape
Computing
Coordinates of control points;
slopes of each vortex segment
Determining coefficient matrix and solve for γ distribution

APPENDIX D

SOLUTION TO A DIFFERENTIAL EQUATION

Equation (14) can be rewritten as

$$\frac{y''}{(1+y'^2)^{3/2}} = \frac{2\gamma_J}{U_\infty C_J} \tag{D.1}$$

where γ_J, U_∞ and C_J are constants.

Let

$$g = y' \tag{D.2}$$

(E.1) becomes

$$\frac{g'}{(1+g^2)^{3/2}} = \frac{2\gamma_J}{U_\infty C_J} \tag{D.3}$$

Integrating both sides of equation (D.3) gives

$$\int \frac{dg}{(1+g^2)^{3/2}} = \frac{2\gamma_J}{U_\infty C_J} \int dx \tag{D.4}$$

thus

$$\frac{g}{(1+g^2)^{1/2}} = \frac{2\gamma_J}{U_\infty C_J} x + K_1 \tag{D.5}$$

where K_1 is determined by letting (D.5) satisfy the initial slope of the distributed vortex segment

$$K_1 = \frac{y'_{oj}}{(1+y'^2_{oj})^{1/2}} - \frac{2\gamma_J}{U_\infty C_J} x_{oj} \cdot \tag{D.6}$$

Equation (D.5) can be solved to yield

$$g = \frac{(\frac{2\gamma_J}{U_\infty C_J} x + K_1)}{[1 - (\frac{2\gamma_J}{U_\infty C_J} x + K_1)^2]^{1/2}} \tag{D.7}$$

Rewriting (D.7) after letting $X = \frac{2\gamma_J}{U_\infty C_J} x + K_1$ and substituting dy/dx for g

$$\frac{dy}{dx} = \frac{X}{(1-X^2)^{1/2}}. \tag{D.8}$$

But

$$dx = \frac{U_\infty C_J}{2\gamma_J} dX, \tag{D.9}$$

then substituting (D.9) into (D.8) and integrating both sides gives

$$y = - \frac{U_\infty C_J}{2\gamma_J} (1-X^2)^{1/2} + K_2. \tag{D.10}$$

The jet deflection can be expressed in term of x as

$$y = - \frac{U_\infty C_J}{2\gamma_J} [1- (\frac{2\gamma_J}{U_\infty C_J} x + K_1)^2]^{1/2} + K_2 \tag{D.11}$$

where K_2, determined by letting (D.11) satisfy the initial location of the distributed vortex segment, is given by

$$K_2 = y_{oj} + \frac{U_\infty C_J}{2\gamma_J} [1 - (\frac{2\gamma_J}{U_\infty C_J} x_{oj} + K_1)^2]^{1/2} \tag{D.12}$$

APPENDIX E

CONVERGENCE OF ITERATIONS

The basic iterative solution consists of two steps.

Step 1

An assumed jet shape is used to evaluate the vortex strength distribution.

Step 2

The vortex strength distribution is used to evaluate the jet shape to be used in the next "Step 1".

Application of this technique produces divergent solutions as illustrated in Fig. 17. An additional step (Step 3) is introduced to produce a modified jet shape for input to Step 1.

Any pair of successive jet shapes form an envelope within which the true shape lies. Because the first assumed jet shape may cross the true shape, it was found to be unwise to take it as a boundary to the envelope. The first envelope is therefore taken as the two jet shapes resulting from the first two applications of Step 2.

Suppose the envelope is bounded by the curves y_1, y_2 (with y_1 above y_2) as on Fig.32. The next input shape is given by

$$y_3 = \frac{1}{2}(y_1 + y_2)$$

and produces the curve y_4 which may lie in any of four regions. The end points are denoted by $(y_4)_{1,\ 2,\ 3,\ 4}$ as shown on Fig. 32 and are used in

the computer programme for determining the input for the next iteration. Consider the four possibilities.

$(y_4)_1$; $(y_4)_1 < y_2$

To produce a curve with $(y_4) < y_2$, the y_3 value would have had to be above y_1 because of the divergent nature of the solutions. Therefore $(y_4)_1$ cannot exist.

$(y_4)_2$; $y_3 < (y_4)_2 < y_2$

Since the iterative solutions diverge, y_3 and $(y_4)_2$ must represent a more restrictive envelope than y_1, y_2 and this new envelope is retained for comparison in the next iteration for which the input is taken as $\frac{1}{2}(y_3 + (y_4)_2)$.

$(y_4)_3$; $y_1 < (y_4)_3 < y_3$

A similar case to $(y_4)_2$. The new envelope is $(y_4)_3$ and y_3 and the input for the next iteration is $\frac{1}{2}(y_3 + (y_4)_3)$.

$(y_4)_4$; $(y_4)_4 < y_1$

In this case, $(y_4)_4$ is outside the original envelope and is rejected. The new envelope is specified by y_1 and y_3 and the next input is $\frac{1}{2}(y_1 + y_3)$.

A similar set of arguments is used if the curve y_2 lies above curve y_1.

APPENDIX F

TREATMENTS OF SINGULAR INTEGRALS

The special treatments of the singular integrals involved in Chapter IV are presented here. There are two typical forms of singular integrations to be dealt, one of which as seen in equation (23) is

$$I_1 = \int_{x_m}^{x_{m+1}} \frac{\ln(1-x)}{x^{3/2}} \frac{x_i - x}{(x_i-x)^2+y_i^2} \, dx \tag{F.1}$$

where the two sets of the limits of the integration used are

$$x_m = 0, \; x_{m+1} = \text{constant}$$

and

$$x_m = \text{constant}, \; x_{m+1} = 1$$

In both cases I_1 is singular at either lower limit $x = 0$ or upper limit $x = 1$. Integrating I_1 by parts,

$$I_1 = \left\{ -2 \left[\frac{(x_i-x)}{(x_i-x)^2 + y_i^2}\right] \left[\ln\left(\frac{1+x^{1/2}}{1-x^{1/2}}\right) + \frac{\ln(1-x)}{x^{1/2}}\right] \right\}_{x_m}^{x_{m+1}} +$$

$$2\int_{x_m}^{x_{m+1}} \left[\ln\left(\frac{1+x^{1/2}}{1-x^{1/2}}\right) + \frac{\ln(1-x)}{x^{1/2}}\right] \frac{[(x_i-x)^2 - y_i^2]}{[(x_i-x)^2 + y_i^2]^2} \, dx \tag{F.2}$$

The integrand in (F.2) is free from singularity at $x_m = 0$ or $x_{m+1} = 1$ and can be calculated fairly accurate by numerical method. Also the first term in the right hand side of equation (F.2) is finite at either limit $x_m = 0$ or $x_{m+1} = 1$ ($\lim_{x\to 0} [\ln(\frac{1+x^{1/2}}{1-x^{1/2}}) + \frac{\ln(1-x)}{x^{1/2}}] = 0$ and $\lim_{x\to 1} [\ln(\frac{1+x^{1/2}}{1-x^{1/2}}) + \frac{\ln(1-x)}{x^{1/2}}] = 2\ln(2)$).

Another form of singular integral also comes from the equation (23) when $y_i = 0$ and $x_m < x_i < x_{m+1}$,

$$I_2 = \int_{x_m}^{x_{m+1}} \frac{\ln(1-x)}{x^{3/2}} \frac{1}{(x_i - x)} dx. \qquad (F.3)$$

I_2 is singular at $x = x_i$ and at either limit of the integration as mentioned above, $x_m = 0$ or $x_{m+1} = 1$.

* The method used to solve this integral is to separate the integrand into additive parts which are either analytically integrable through the singularity or have no singularity (and hence can be solved accurately enough by numerical method). In this case the integrand is rearranged so that

$$I_2 = \int_{x_m}^{x_{m+1}} F_{(x)} dx + \frac{1}{x_i} \int_{x_m}^{x_{m+1}} \frac{\ln(1-x)}{x^{3/2}} dx + \frac{1}{x_i(x_i-1)} \int_{x_m}^{x_{m+1}} \ln(1-x)dx + \frac{\ln(1-x_i)}{x_i^{3/2}} \int_{x_m}^{x_{m+1}} \frac{1}{x_i - x} dx \qquad (F.4)$$

*This particular solution is proposed by B. Mc Donald, Department of Electrical Engineering, University of Manitoba.

with

$$F_{(x)} = \frac{\left[\frac{\ln(1-x)}{x^{3/2}} - \frac{\ln(1-x_i)}{x_i^{3/2}}\right]}{(x_i-x)} - \frac{\ln(1-x)}{x_i}\left[\frac{1}{x^{3/2}} + \frac{1}{x_i-1}\right] \qquad (F.5)$$

Direct integration of the last three terms of (F.4) gives

$$\int_{x_m}^{x_{m+1}} \frac{\ln(1-x)}{x^{3/2}} = -2\left[\ln\left(\frac{1+x^{1/2}}{1-x^{1/2}}\right) + \frac{\ln(1-x)}{x^{1/2}}\right]\Bigg|_{x_m}^{x_{m+1}} \qquad (F.6)$$

$$\int_{x_m}^{x_{m+1}} \ln(1-x)dx = x\ln(x) - x\Big|_{x_m}^{x_{m+1}} \qquad (F.7)$$

$$\int_{x_m}^{x_{m+1}} \frac{1}{x_i-x}\,dx = -\ln(x_i-x)\Big|_{x_m}^{x_i} - \ln(x-x_i)\Big|_{x_i}^{x_{m+1}} \qquad (F.8)$$

(F.6), (F.7) and (F.8) are finite at either limit $x_m = 0$ or $x_{m+1} = 1$.

Application of l'Hopital rule to the first term of $F_{(x)}$ allows the determination of $F_{(x)}$ at $x = x_i$,

$$F_{(x_i)} = \frac{1}{x_i^{3/2}(1-x_i)} + \frac{3}{2}\frac{\ln(1-x_i)}{x_i^{5/2}} - \frac{\ln(1-x_i)}{x_i}\left[\frac{1}{x_i^{3/2}} + \frac{1}{x_i-1}\right] \qquad (F.9)$$

The value of F(x) at x = 0, x = 1 is determined by rearranging F(x) in the form

$$F_{(x)} = \frac{\ln(1-x)}{x_i}\left[\frac{1}{x^{1/2}(x_i-x)} - \frac{1}{x_i-1}\right] - \frac{\ln(1-x_i)}{x_i^{3/2}(x_i-x)}. \qquad (F.10)$$

Again applying l'Hopital rule to determine F(0) and F(1) from (F.10),

$$F(0) = - \frac{\ln(1-x_i)}{x_i^{5/2}} \tag{F.11}$$

and

$$F(1) = - \frac{\ln(1-x_i)}{x_i^{3/2}(x_i-1)} \tag{F.12}$$

APPENDIX G

REPRESENTATION OF STRAIGHT UNIFORM JET

Kuchemann and Weber in Reference 7 showed that two semi-infinite plane parallel vortex sheets are equivalent to a source distribution and a strip of uniform flow. This principle will be used to represent a straight uniform jet. It will be shown below that the velocity field resulting from the superimposing of the velocity fields of two parallel vortex sheets and a source distribution in a two dimensional plane produces a straight uniform jet.

Induced Velocities by Two Vortex Distributions

Consider two semi infinite plane parallel uniform vortex distribution of strengths γ and $-\gamma$ on two lines $y=-\frac{\delta}{2}$ and $y=\frac{\delta}{2}$ as shown in Fig.30.From equation (B.9) the horizontal components of velocities induced by the parts of vortex sheets 1 and 2 which stretch from x=0 to x_{A_1} and x_{A_2} (Fig.30) are respectively

$$u_{i-1} = -\frac{\gamma}{2\pi}(\phi_{11} - \phi_1) \qquad (G.1)$$

and

$$u_{i-2} = \frac{\gamma}{2\pi}(\phi_{22} - \phi_2) \qquad (G.2)$$

Adding (G.1) and (G.2) yields

$$u_{i-1} + u_{i-2} = \frac{\gamma}{2\pi}[(\phi_1 - \phi_2) - (\phi_{11} - \phi_{22})] \qquad (G.3)$$

At the limit when x_{A_1} and x_{A_2} go to infinity,

$$\phi_{11} = \phi_{22} = \pi, \tag{G.4}$$

and (G.3) becomes

$$u_{i-1} + u_{i-2} = \frac{\gamma}{2\pi} (\phi_1 - \phi_2) \tag{G.5}$$

Similarly, from equation (B.8) the vertical components of velocities induced by the parts of vortex sheets 1 and 2 previously considered can be found and their sumation is

$$v_{i-1} + v_{i-2} = \frac{\gamma}{2\pi} (\ln \frac{r_{22}}{r_2} - \ln \frac{r_{11}}{r_1}). \tag{G.6}$$

At the limit when x_{A_1} and x_{A_2} go to infinity, r_{11} is equal to r_{22} and (G.6) becomes

$$v_{i-1} + v_{i-2} = \frac{\gamma}{2\pi} \ln (\frac{r_1}{r_2}) \tag{G.7}$$

Induced Velocities by a Source Distribution

Consider a two dimensional uniform source distribution of strength q on the y axis between $y = -\frac{\delta}{2}$ and $y = \frac{\delta}{2}$ as shown in Fig.31 The two components of induced velocity are

$$u_s = \frac{q}{2\pi} \int_{-\frac{\delta}{2}}^{\frac{\delta}{2}} \frac{\sin\theta}{r} dy \tag{G.8}$$

and

$$v_s = \frac{q}{2\pi} \int_{-\frac{\delta}{2}}^{\frac{\delta}{2}} \frac{\cos\theta}{r} \, dy \tag{G.9}$$

where subscript s indicates the source.

But

$$\tan \theta = \frac{x_i}{y_i - y} \tag{G.10}$$

differentiate both sides of (G.10) with respect to θ and y,

$$\frac{d\theta}{\cos^2\theta} = \frac{x_i}{(y_i - y)^2} \, dy \tag{G.11}$$

Also

$$r^2 = x_i^2 + (y_i - y)^2, \tag{G.12}$$

thus

$$2rdr = -2 \, (y_i - y) \, dy \tag{G.13}$$

Using (G.11) and (G.13) to change the variables in the integration of equations (G.8) and (G.9) respectively,

$$u_s = \frac{q}{2\pi} \int_{\theta_2}^{\theta_1} \frac{\sin\theta}{r} \frac{(y_i - y)^2}{x_i} \frac{1}{\cos^2\theta} \, d\theta, \tag{G.14}$$

or

$$u_s = \frac{q}{2\pi} \int_{\theta_2}^{\theta_1} d\theta = \frac{q}{2\pi} \, (\theta_1 - \theta_2) \, , \tag{G.15}$$

and

$$v_s = \frac{q}{2\pi}\int_{r_2}^{r_1} \frac{\cos\theta}{r}\left(-\frac{r}{y_i - y}\right) dr \qquad (G.16)$$

or

$$v_s = \frac{q}{2\pi}\int_{r_2}^{r_1} -\frac{dr}{r} = -\frac{q}{2\pi}\ln\left(\frac{r_1}{r_2}\right) \qquad (G.17)$$

Total Induced Velocities by Previous Two Vortex Distributions and the Source Distribution

Assuming the vortex and the source strength per unit length are equal or

$$\gamma = q \qquad (G.18)$$

The total induced velocities are defined as

$$u_{total} = (u_{i-1} + u_{i-2}) + u_s \qquad (G.19)$$

and

$$v_{total} = (v_{i-1} + v_{i-2}) + v_s \qquad (G.20)$$

Substituting (G.5) and (G.15) into (G.19) and also applying (G.18),

$$u_{total} = \frac{\gamma}{2\pi}[(\phi_1 - \phi_2) + (\theta_1 - \theta_2)], \qquad (G.21)$$

and v_{total} is readily seen to vanish.

It is desired now to observe the velocity field in some particular regions.

At $x = -\infty$	$u_{total} = 0$	
At $x = 0+$	$u_{total} = 0$	for $\lvert y\rvert > \delta/2$
	$u_{total} = \gamma$	for $\lvert y\rvert < \delta/2$
At $x = +\infty$	$u_{total} = 0$	for $\lvert y\rvert > \delta/2$
	$u_{total} = \gamma$	for $\lvert y\rvert < \delta/2$

The resulting flow is a parallel flow in the region between the lines $y = y_o$, $y = -y_o$ and for $x > 0$, with constant velocity, $v = \gamma$ or q.

REFERENCES

1. Davidson, M. , "The Jet Flap", Journal of The Royal Aeronautical Society, Vol.60, Jan 1956, p.25.
2. Spence, D. A. , "The Lift Coefficient of a Thin Jet-Flapped Wing", Proc. Roy. Soc. (London), ser. A, pp. 46-68, Dec.4,1956.
3. Spence, D. A. , "The Lift on a Thin Aerofoil with a Jet-Augmented Flap", Aeronautical Quarterly, Vol.9, pt.3, 1958.
4. Whittley, D. C. , "The Augmentor Wing: A New Means of Engine Airframe Integration for STOL Aircraft", Fourth ICAS Conference, Paris, 1964, AIAA paper No. 64-574.
5. Chan, Y. Y. , "The Lift on a Two-Dimensional Augmentor Wing", NRC Aeronautical Report, LR-523, April 1969.
6. Mises, R. V. , "Theory of Flight", Dover Publications, Inc., 1959.
7. Kuchemann and Weber, "Aerodynamics of Propulsion", Mc Graw-Hill, 1953.
8. Dimmock, N. A. 1955 Unpublished Ministry of Supply Report
9. Herold, A. C. , "A Two Dimensional, Iterative Solution for the Jet Flap", NASA Contractor Report, NASA CR-2190, February 1973

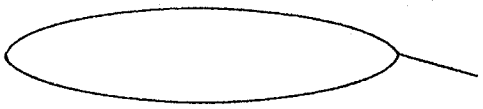

Fig. 1 . Model of Elliptic Wing
with Mechanical Flap

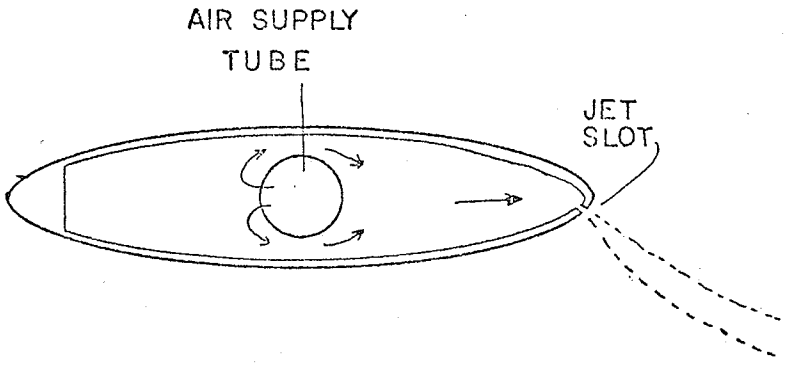

Fig. 2 . Model of Elliptic Wing
with Jet Flap

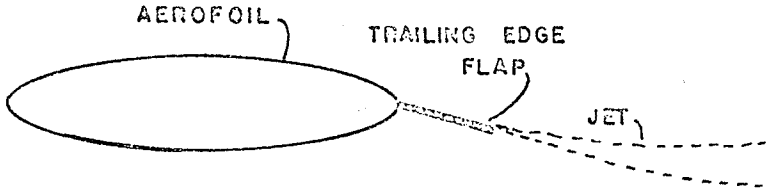

Fig. 3. Model of Elliptic Wing with Jet-Augmented Flap

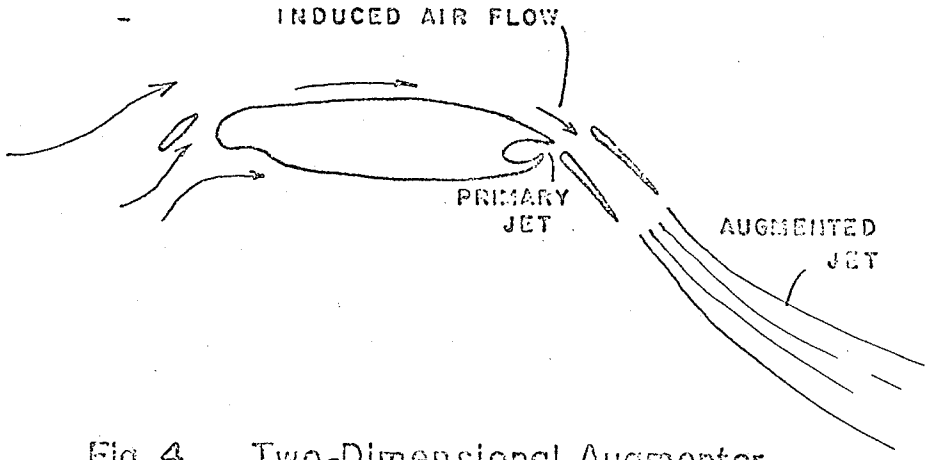

Fig. 4. Two-Dimensional Augmentor Wing

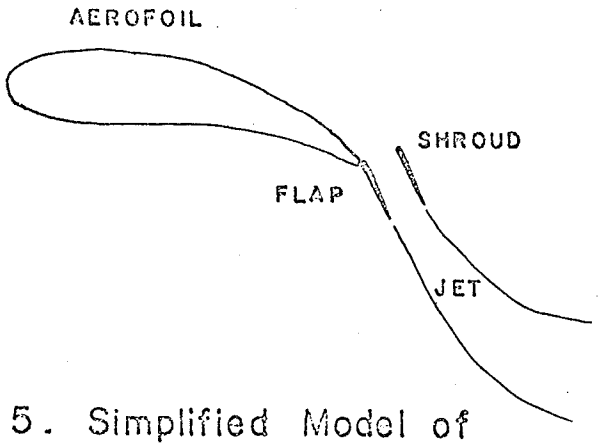

Fig. 5. Simplified Model of Augmentor Wing

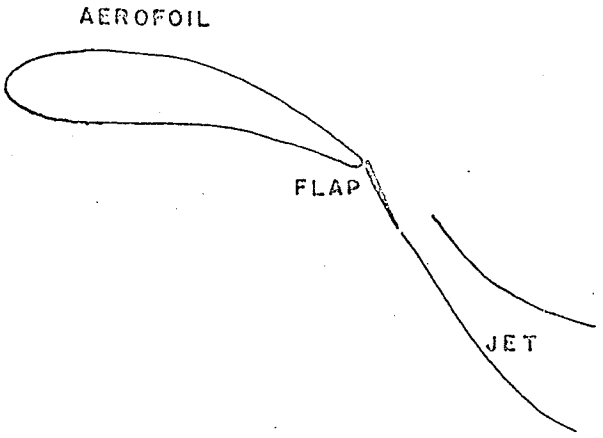

Fig. 6. Simplified Model of Augmentor Wing without Shroud

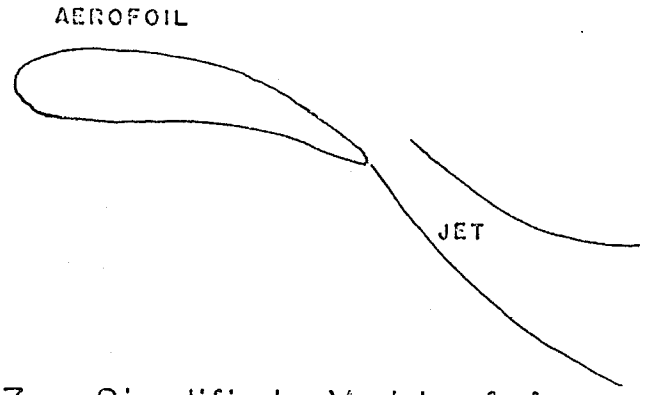

Fig.7. Simplified Model of Augmentor Wing without Flap and Shroud

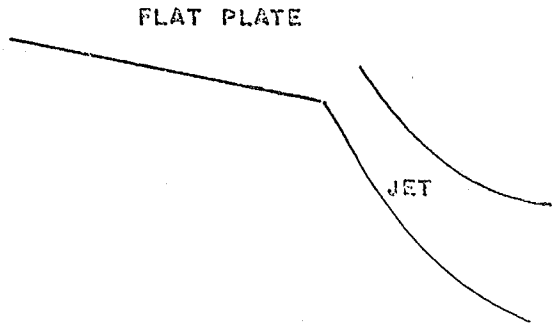

Fig.8. Final Model of Augmentor Wing

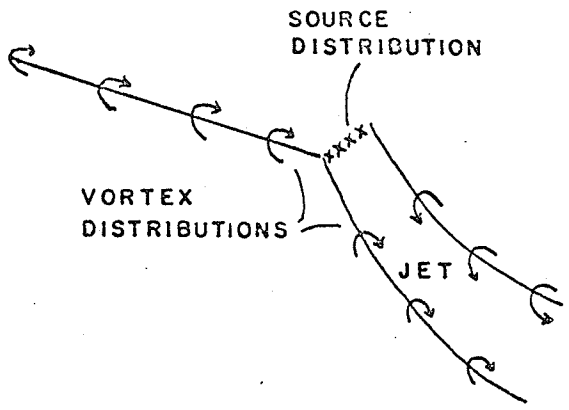

Fig. 9. Hypothetical Model of Augmentor Wing

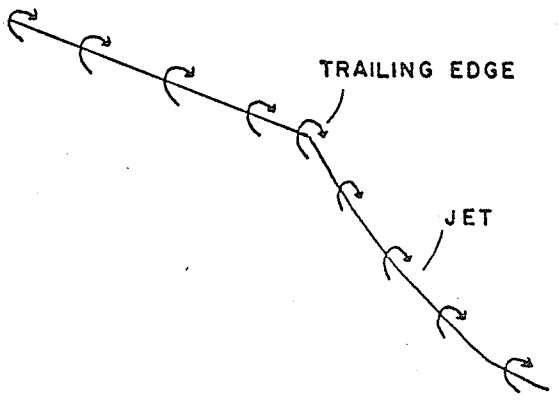

Fig. 10. Model of Jet Flap

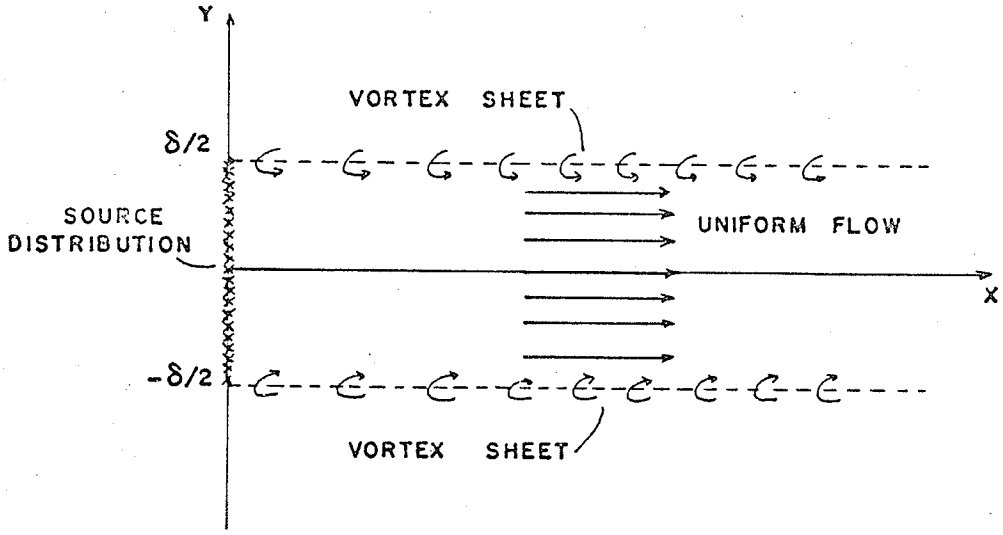

Fig. 11. Straight Uniform Jet resulting from Vortex Sheets and a Source Distribution

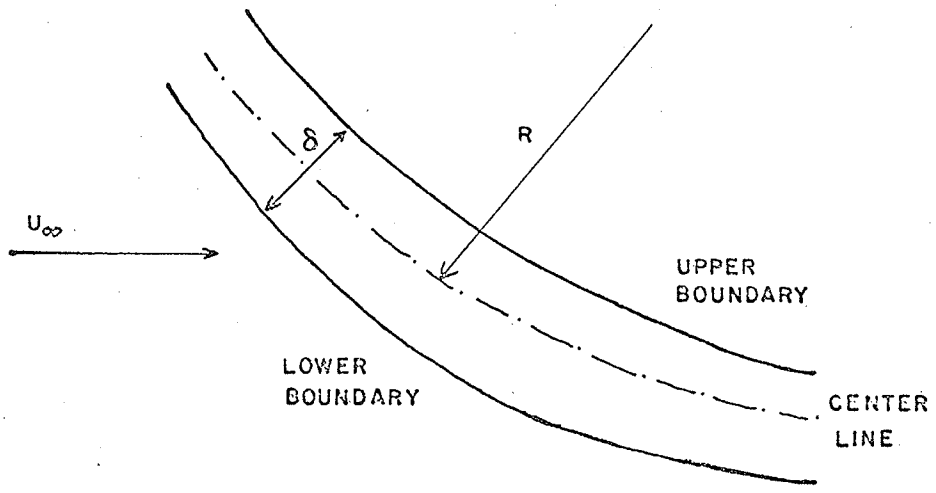

Fig. 12. Two-Dimensional Jet

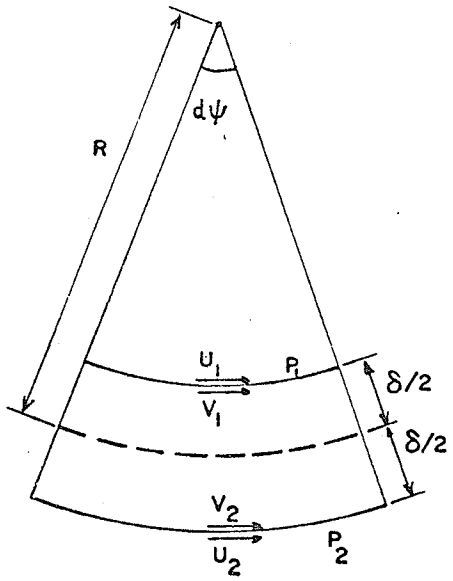

Fig. 13. Polar Element of Curve Jet

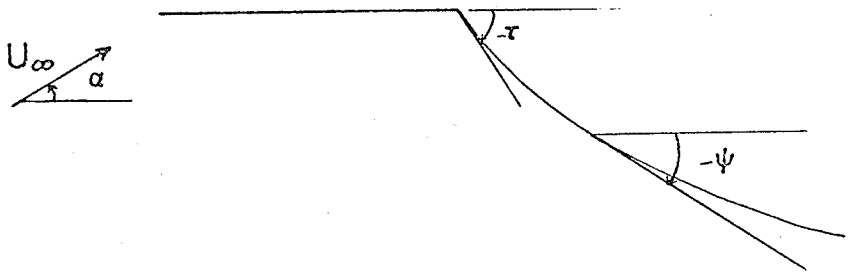

Fig. 14. Aerofoil and Jet as Boundaries

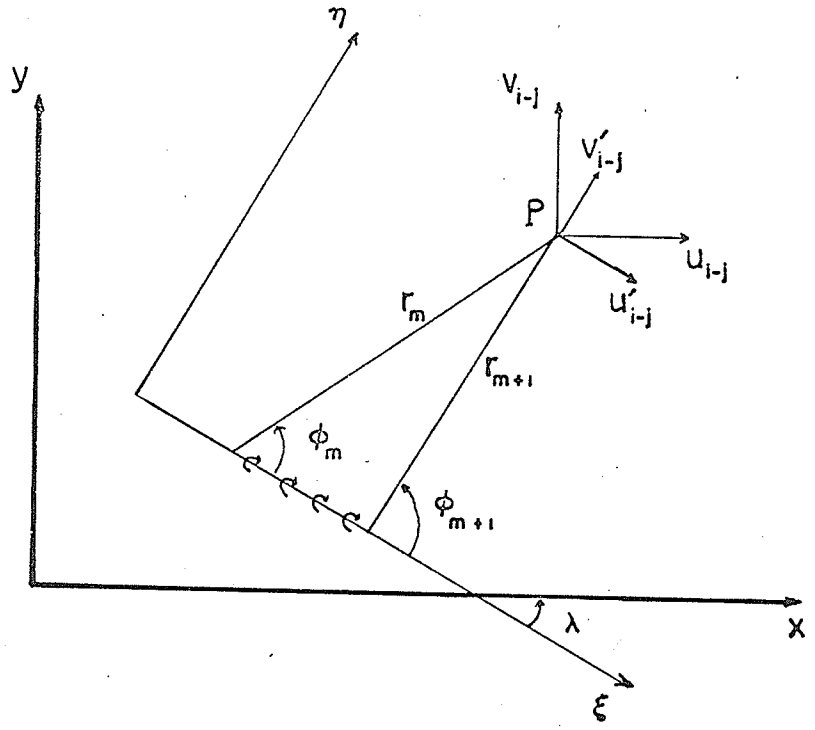

Fig. 15. Induced Velocities by a Vortex Element

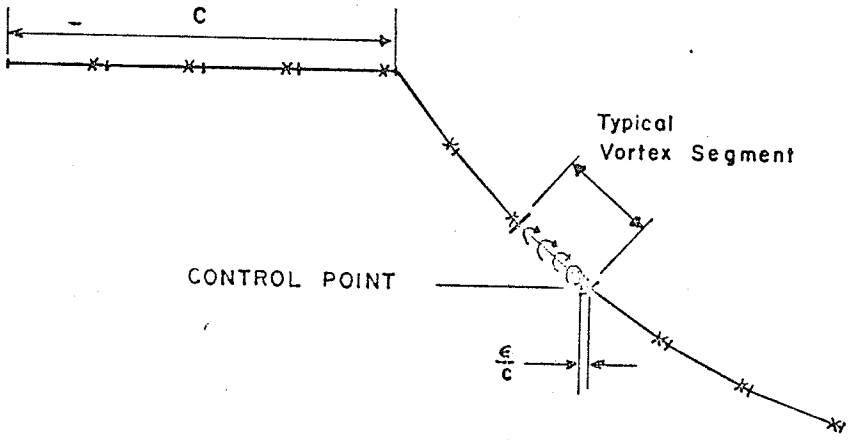

Fig. 16. Control Points and Segments of Vortex Distribution

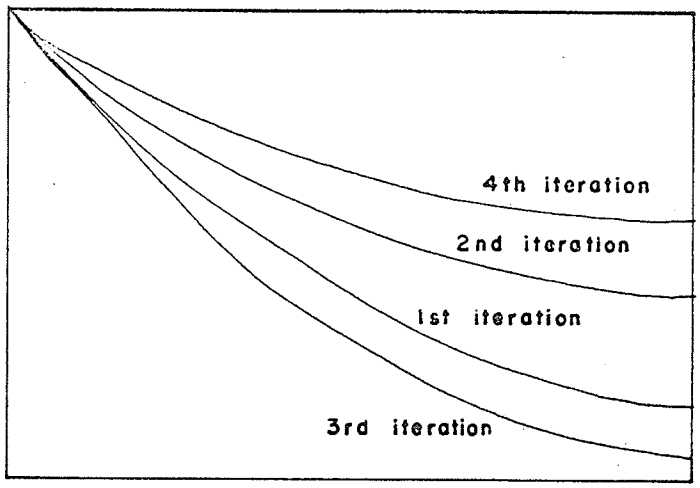

Fig. 17. Illustrated Jet Shapes after four Normal Iterative Steps

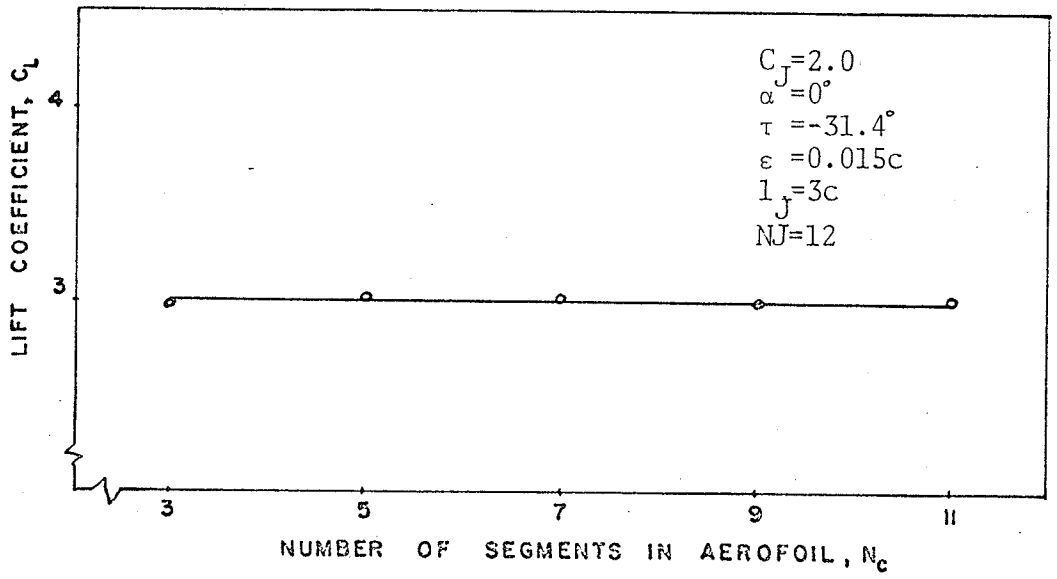

Fig. 18. Effect of Number of Segments in Aerofoil on Lift Coefficient

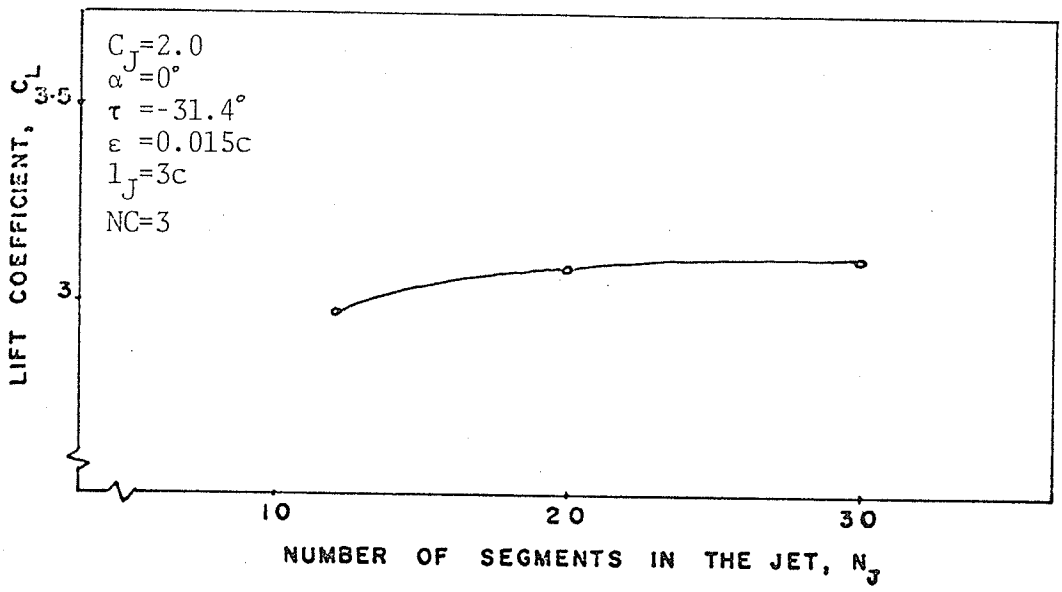

Fig. 19. Effect of Number of Segments in The Jet on Lift Coefficient

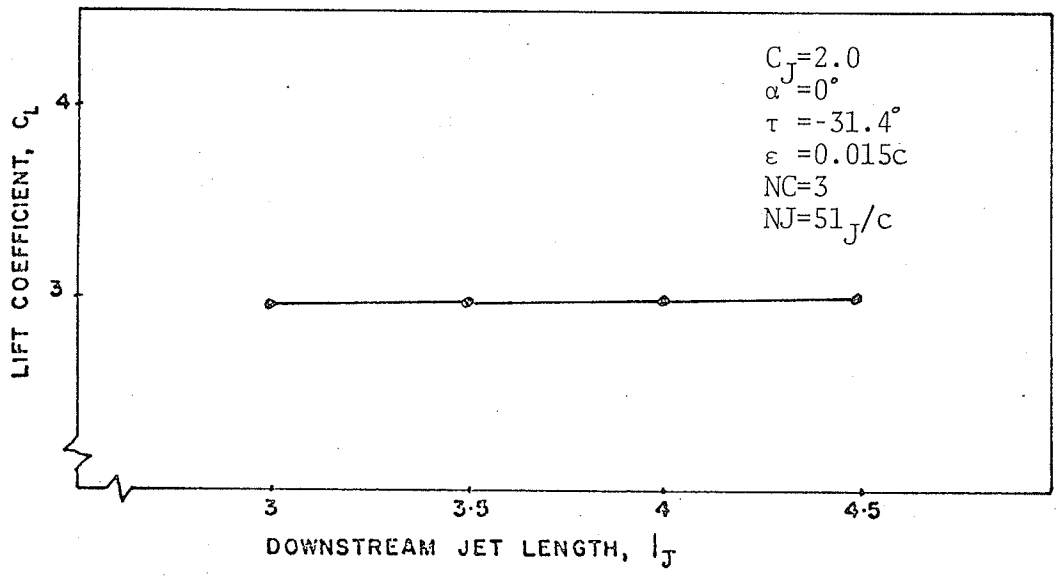

Fig. 20. Effect of Jet Length on Lift Coefficient

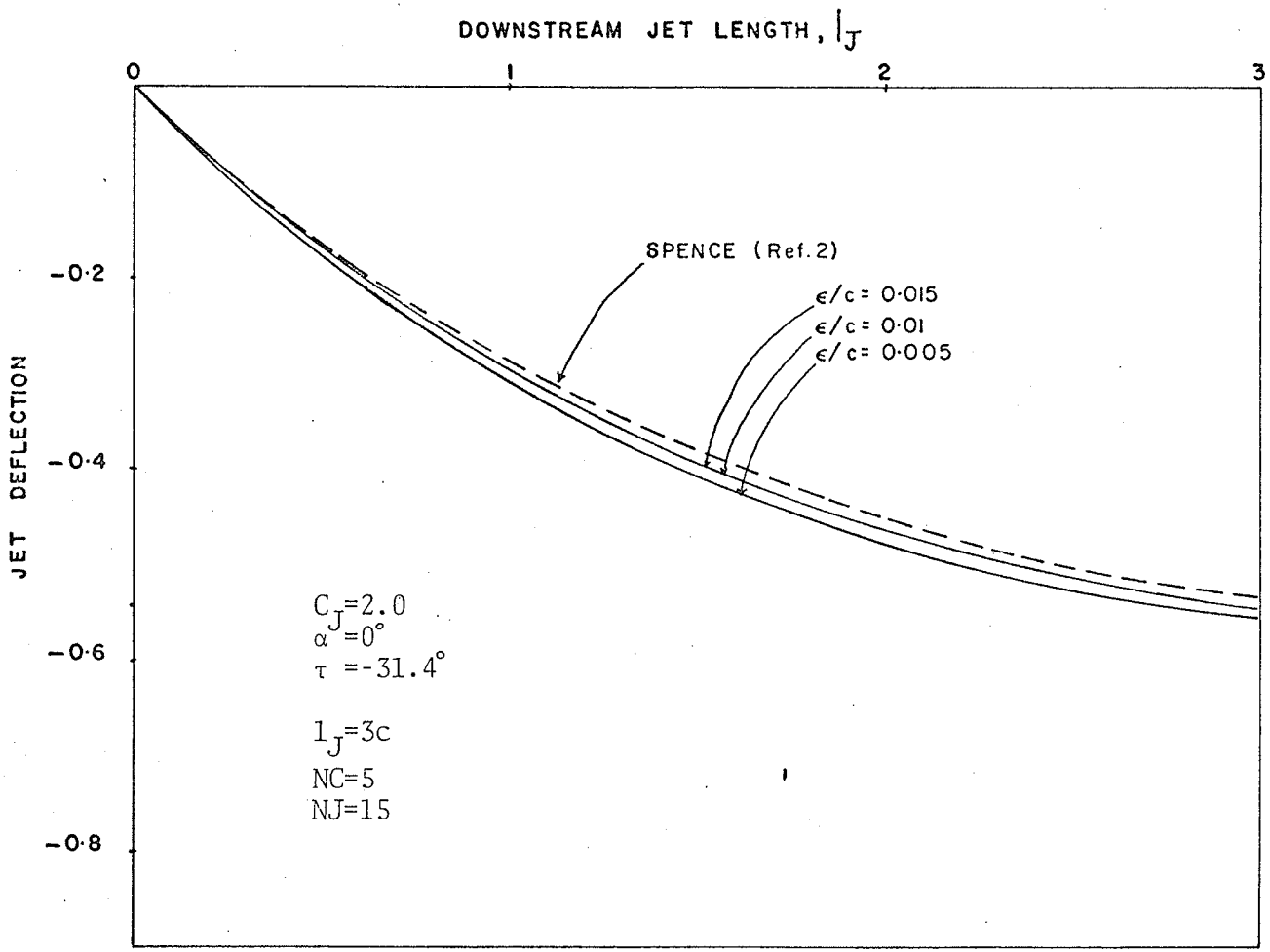

Fig. 21. Effect of Positions of Control Points on Jet Shape

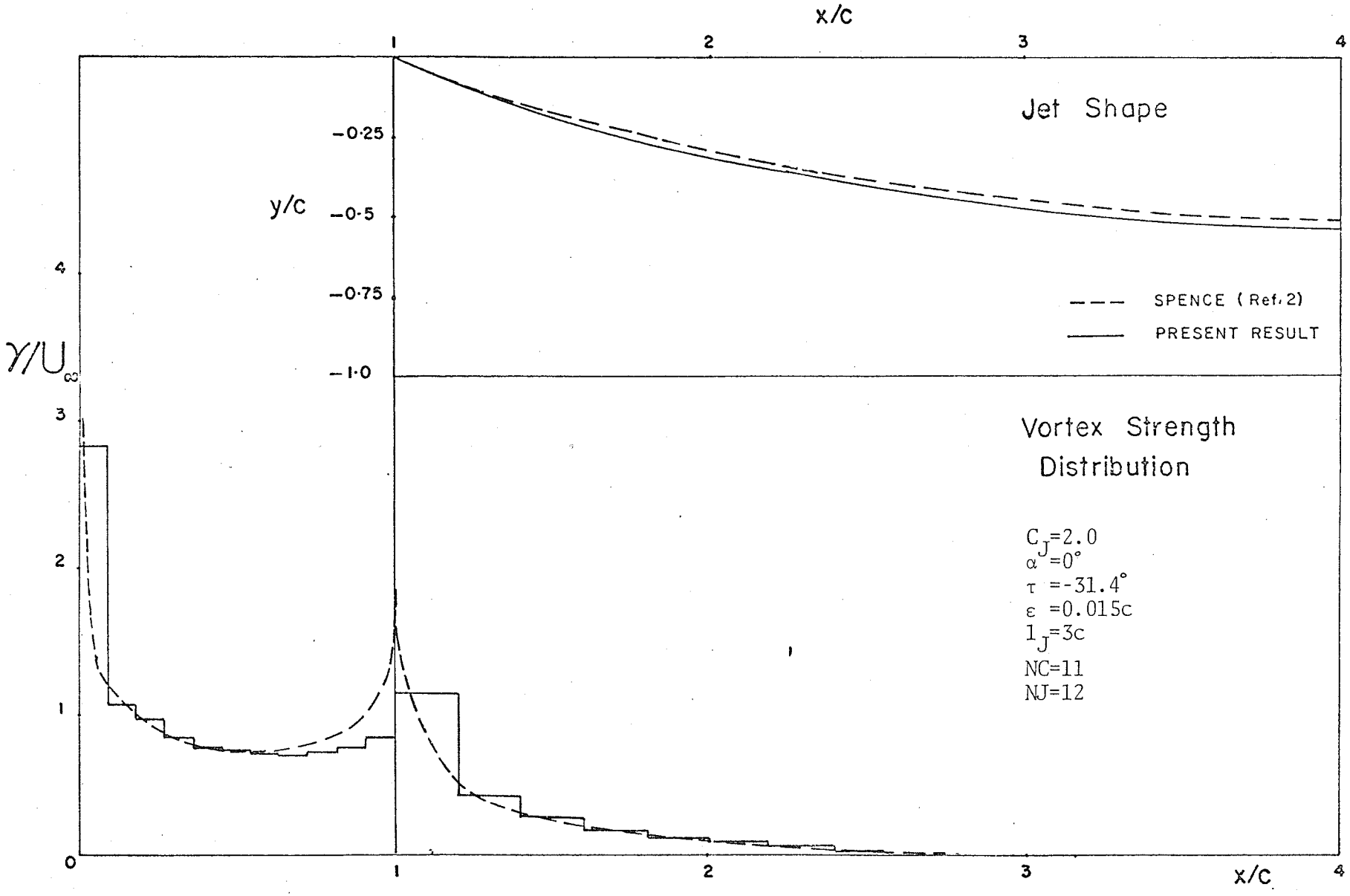

Fig. 22, Step Vortex Strength Distribution and Jet Shape (C_J=2·0)

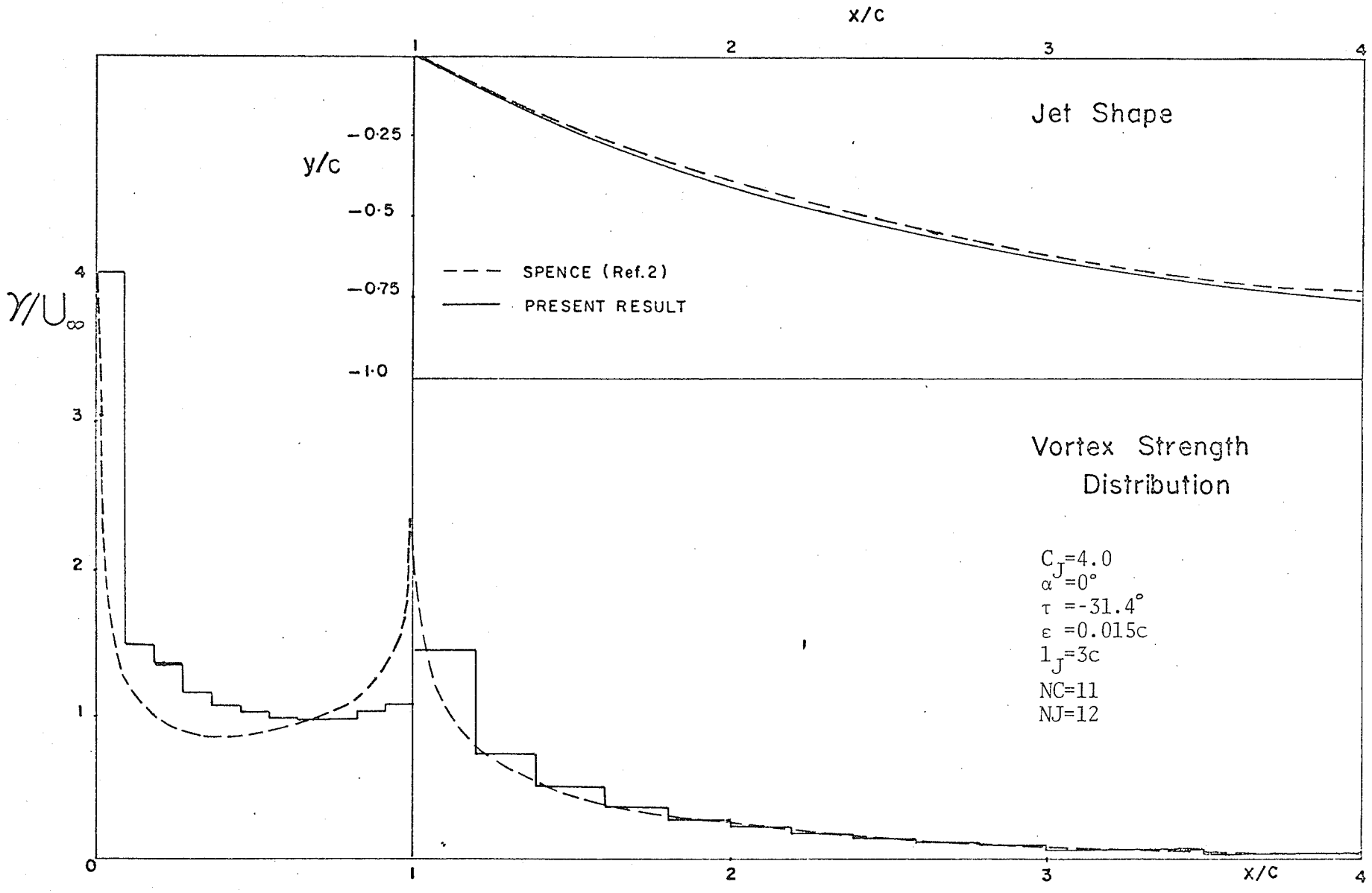

Fig. 23. Step Vortex Strength Distribution and Jet Shape (C_J=4·0)

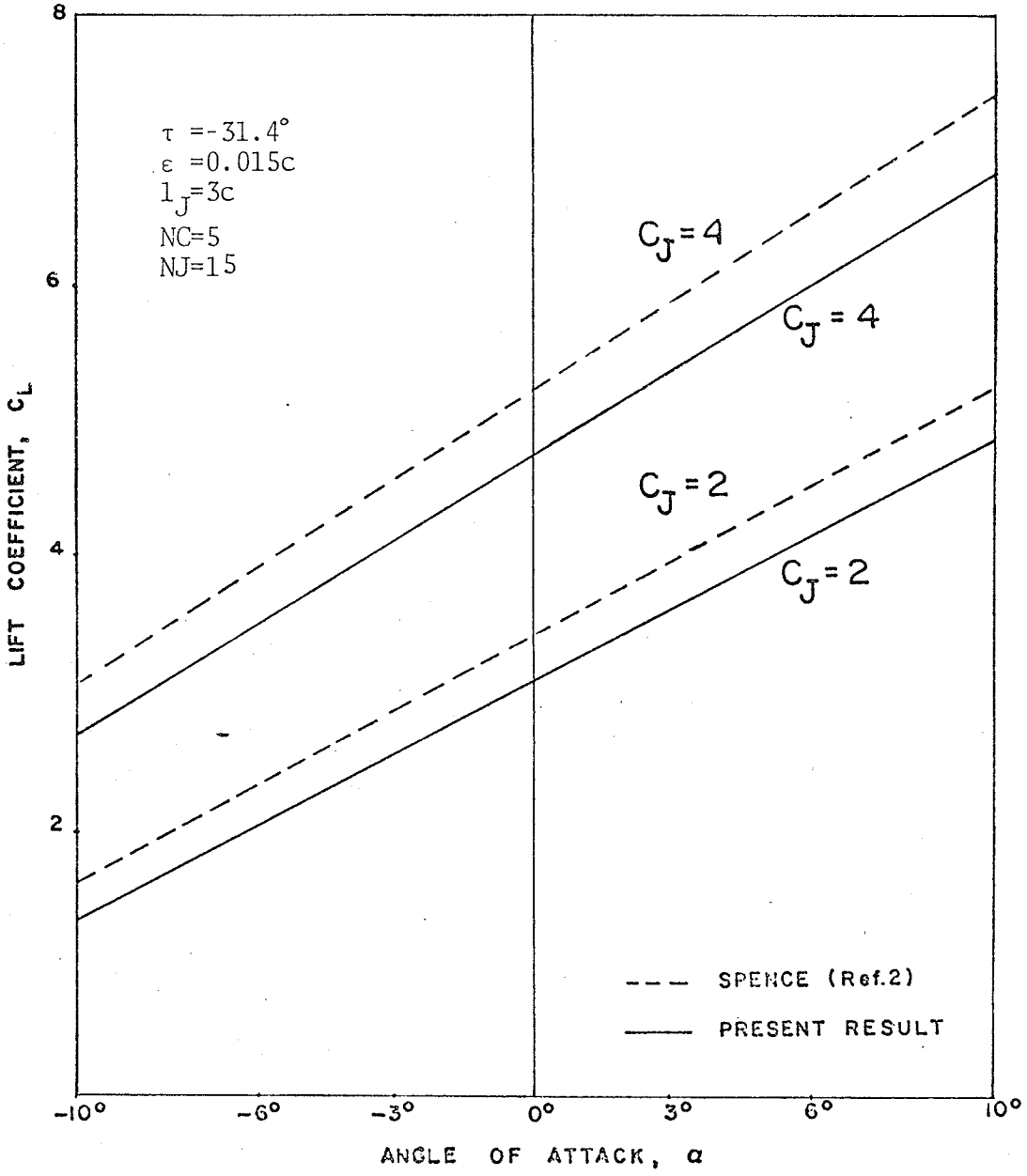

Fig.24. - Lift Coeffient and the Attack Angle (STEP METHOD)

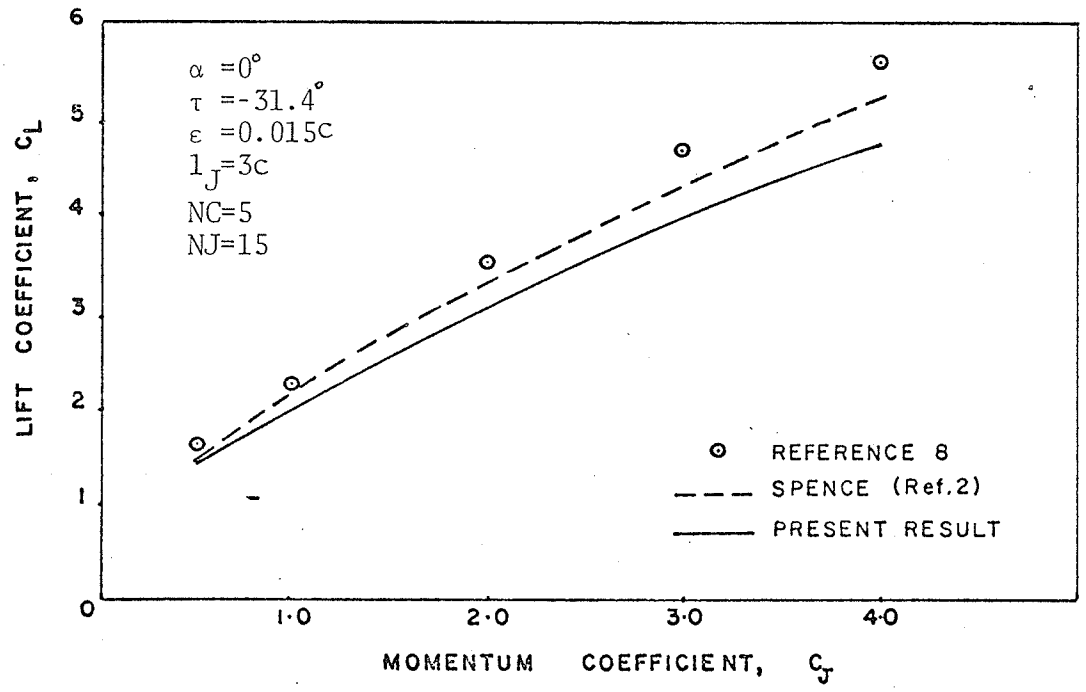

Fig.25. Lift Coeffient versus Momentum Coefficient (STEP METHOD)

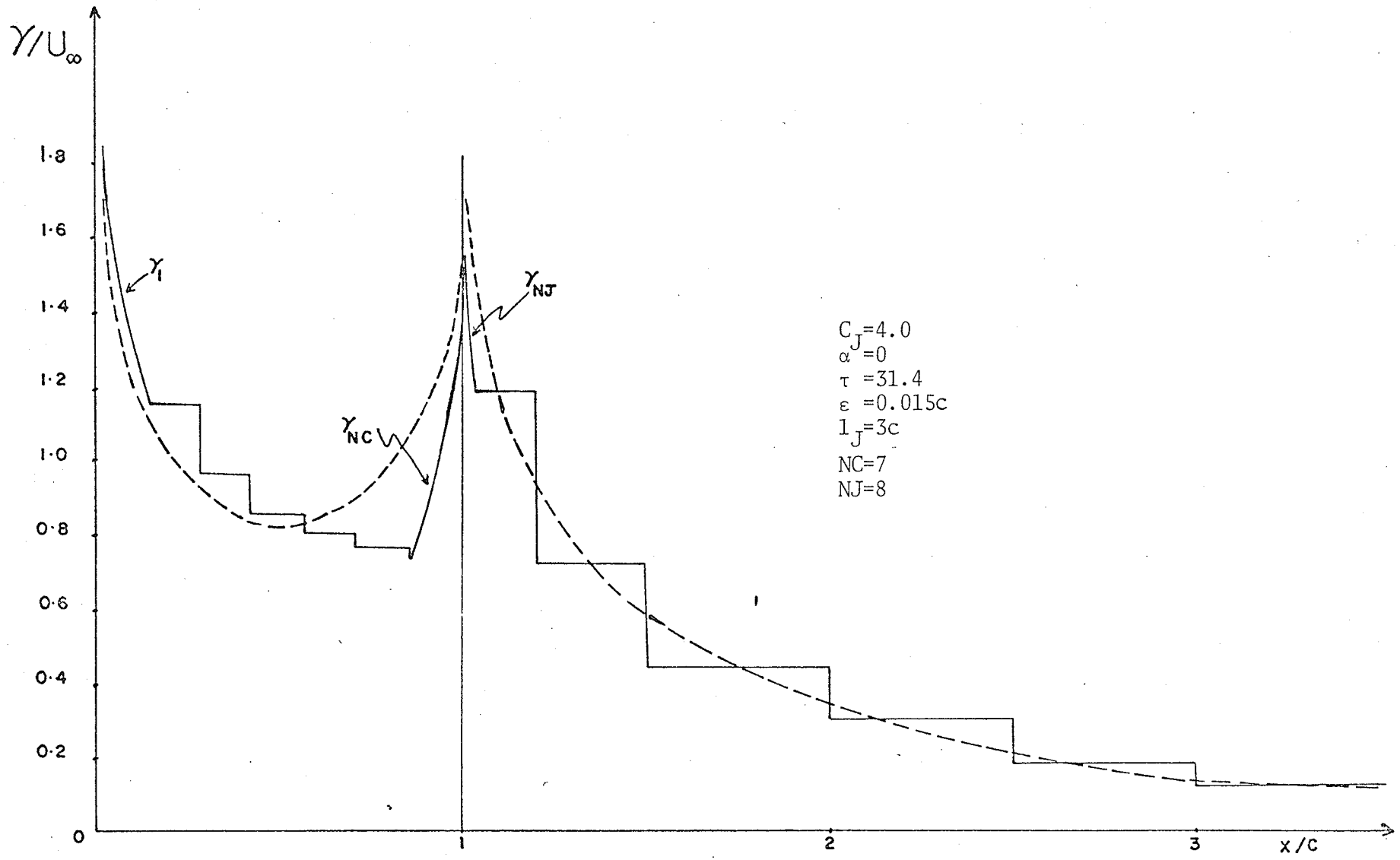

Fig. 26. Modified Step Vortex Strength Distribution (C_J = 4·0)

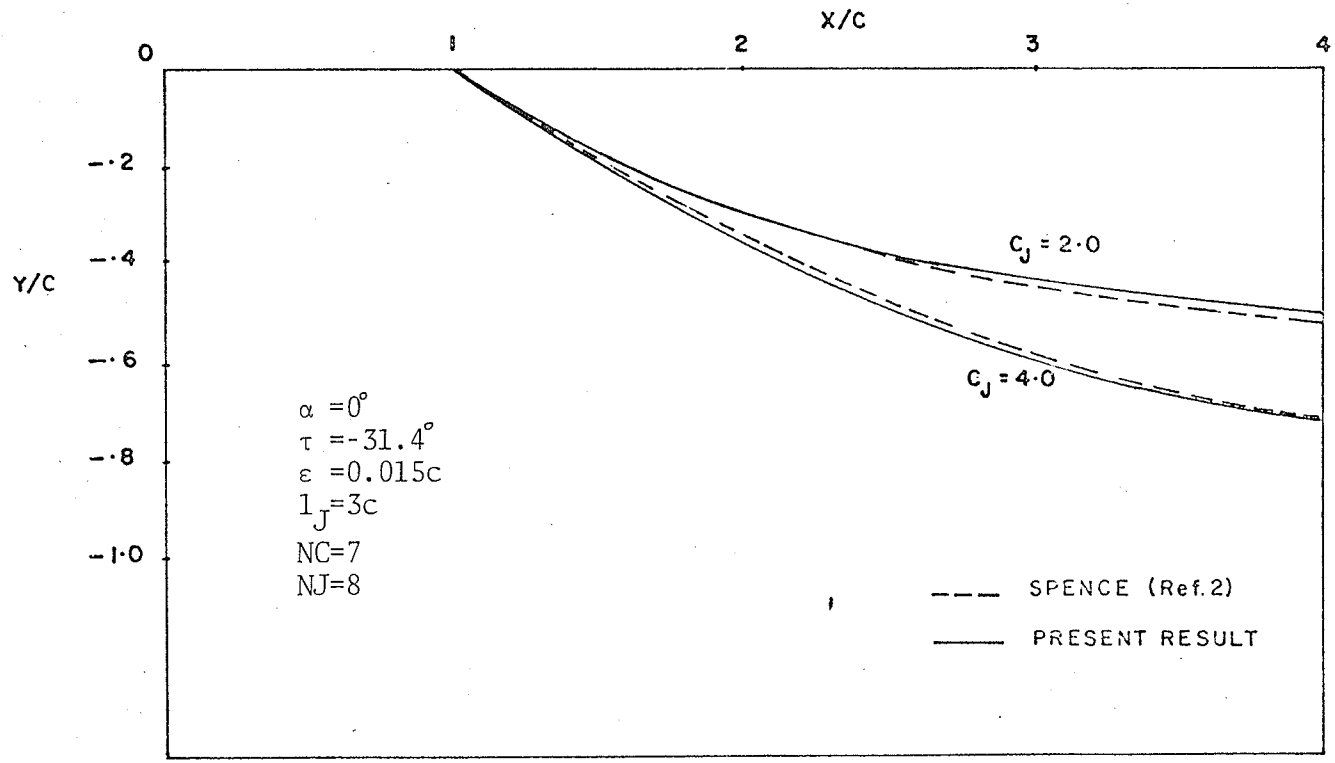

Fig. 27. Jet Shape (MODIFIED STEP METHOD)

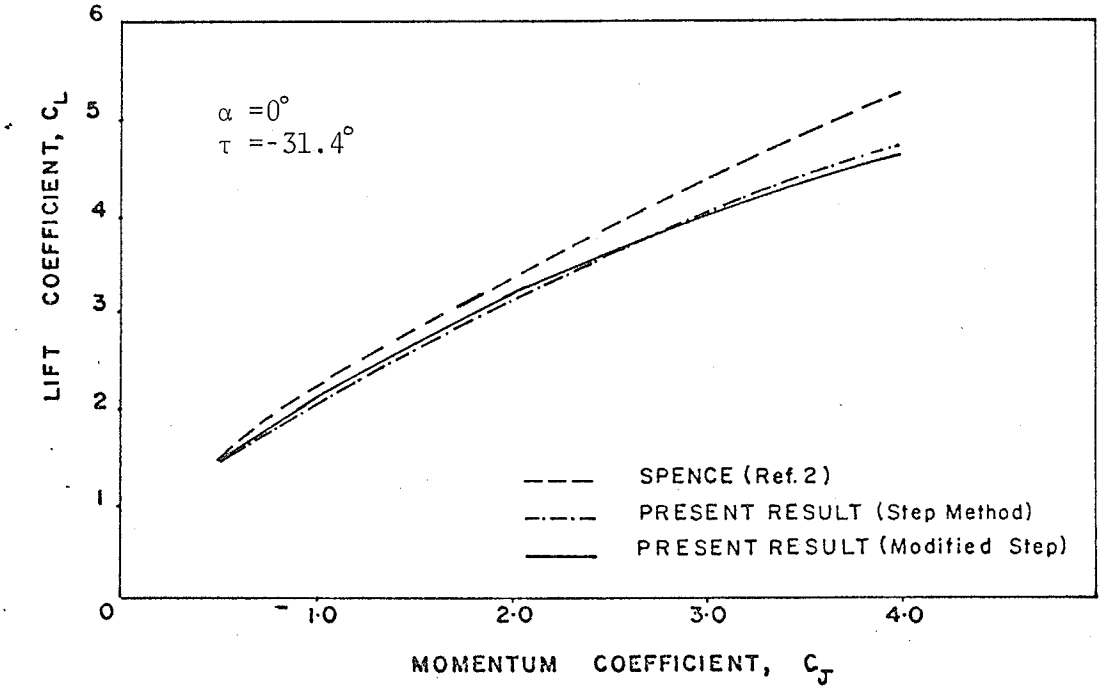

Fig.28. Lift Coefficient versus Momentum Coefficient

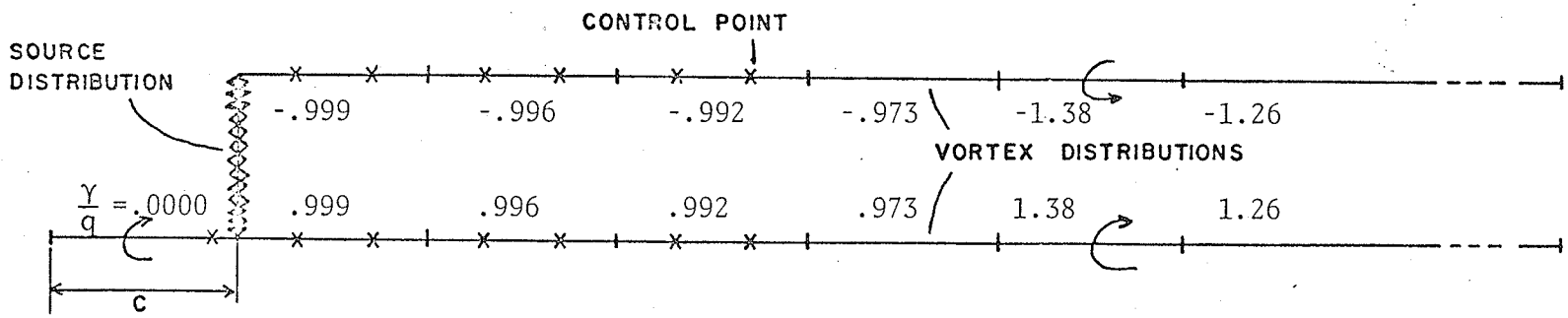

Fig. 29. Flat Plate Aerofoil with Straight Thick Jet

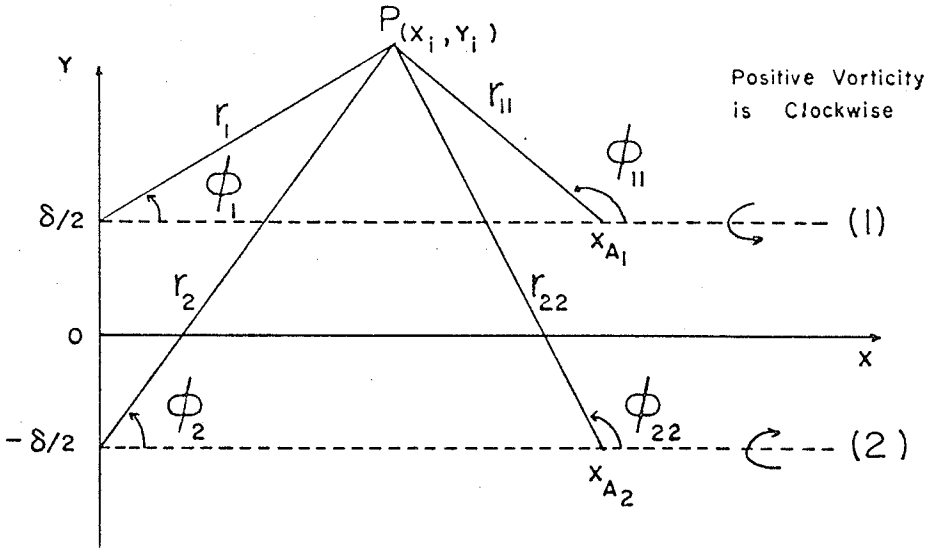

Fig.30 Two Semi Infinite Plane Parallel Vortex Sheets

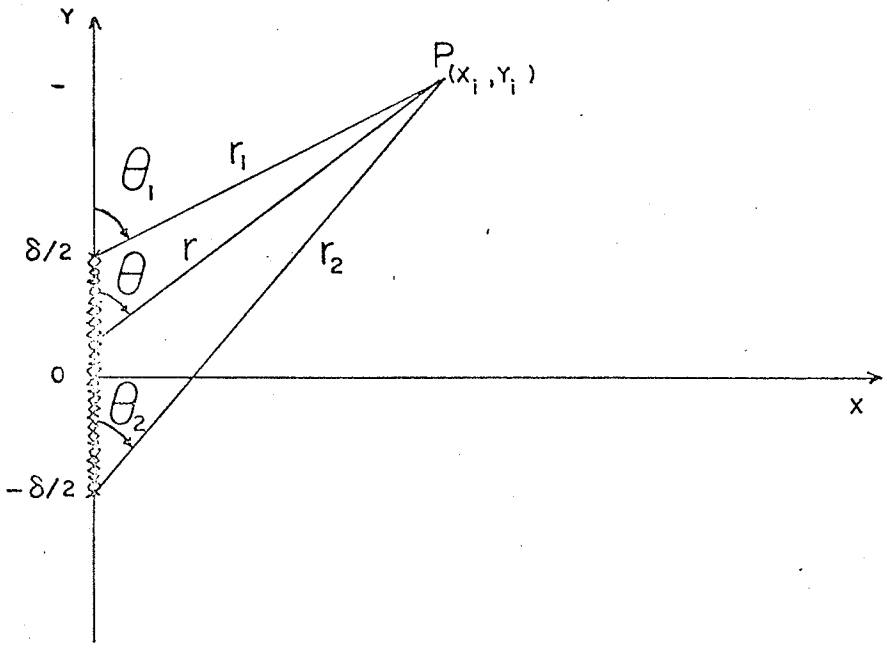

Fig. 31. Uniform Source Distribution

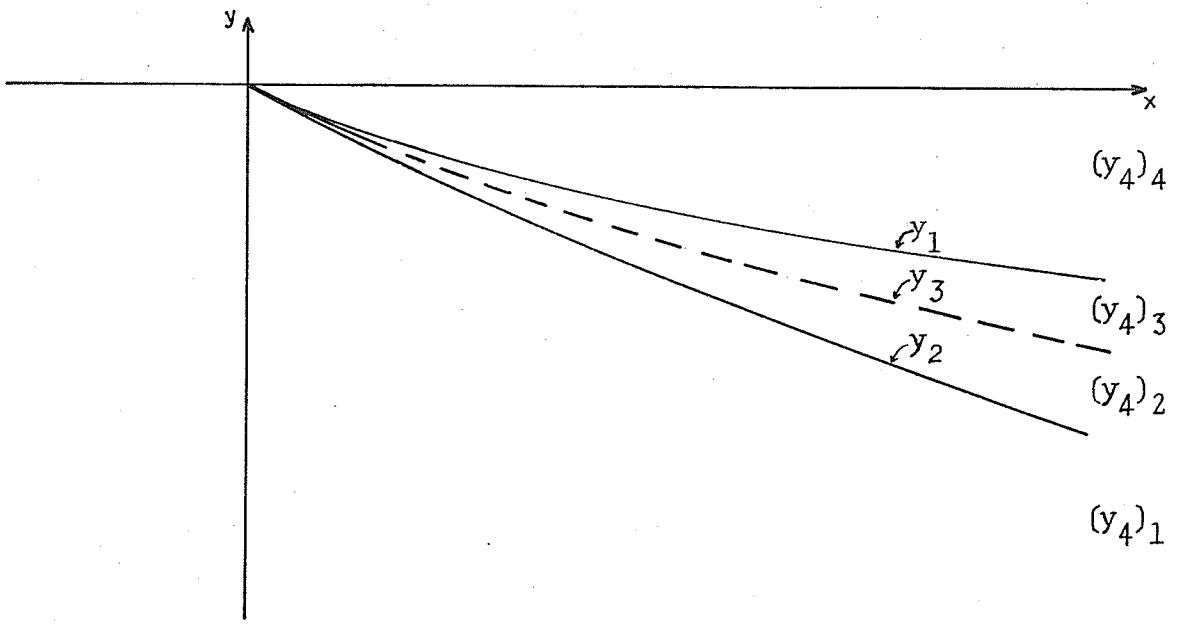

Fig. 32. Specified Regions of Jet Shapes